

FINITE ELEMENT ANALYSIS OF SHIP-ICE COLLISION
USING LS-DYNA

RUI ZONG



FINITE ELEMENT ANALYSIS OF SHIP-ICE COLLISION
USING LS-DYNA

By

© Rui Zong

A thesis submitted to the
School of Graduate Studies
in partial fulfillment of the requirements for the degree of
Master of Engineering

Faculty of Engineering and Applied Science
Memorial University of Newfoundland

July 2012

St. John's

Newfoundland

ABSTRACT

The energy industry's increasing interest in the Arctic region demands more and stronger polar ships. IACS has released a set of documents titled Unified Requirements for Polar Ships (URI) to harmonize different ice classification specifications. This thesis defines a procedure for evaluating an "IACS Polar Class" ship under ice impacts using LS-DYNA, an explicit finite element analysis tool. The final product includes a numerical model that is capable of evaluating the global motions of the ship and ice, the ship-ice contact force, and the local structural response of the ship. A few ice material models whose pressure-area relationships comply with the URI are proposed as well. Restoring forces are modeled using user-defined-curve-functions. This innovative approach significantly reduces the computation cost by excluding the water domain from the analysis. The Arbitrary Lagrangian-Eulerian method in LS-DYNA is discussed and employed to estimate necessary inputs for the user-defined-curve-functions. Several ship-ice impact scenarios are modeled in LS-DYNA and contact forces are compared with the estimations by DDePS, a simple analytical solution that is consistent with the URI. In the last part of this thesis, the ship from the previous analysis is ice-strengthened with internal structures in accordance with the URI and the DNV specifications. Local structural response of this ship under ice impacts is assessed.

ACKNOWLEDGEMENTS

To begin with this thesis, I would like to express my sincerest appreciation to my supervisor Dr. Claude Daley for his excellent support, direction, and guidance. I am also thankful to STEPS2 and NSERC CREATE program for their generous financial support.

This thesis would be impossible without the help and support from a few great people. I would also like to state my great gratitude to the following:

Dr. Wei Qiu, professor at MUN, for bringing me to this outstanding university.

Dr. Bruce Colbourne, professor at MUN, for all the insightful and inspiring discussions throughout my research.

Mr. Bruce Quinton, a fellow graduate student at my office, for your wonderful help and patience.

Dr. Junyong Wang and Dr. Rober Gagnon at NRC-IOT, for your remarkable help.

Lastly, I would like to thank my family and my girlfriend for your unconditional support. This thesis is dedicated to you.

Table of Contents

ABSTRACT.....	ii
ACKNOWLEDGEMENTS.....	iii
Table of Contents.....	iv
List of Tables.....	xi
List of Figures.....	xiv
List of Nomenclature or Abbreviations.....	xviii
List of Appendices.....	xx
Chapter 1 Introduction.....	1
1.1 Scope and Objectives.....	2
1.2 Thesis Organization.....	3
1.3 LS-DYNA.....	5
1.3.1 General Information.....	5
1.3.2 Time Step Control and Total Time Cost.....	7
1.3.3 The Arbitrary Lagrangian-Eulerian (ALE) Method.....	9
1.3.4 Contact Model.....	12
1.3.5 User Defined Curve Function.....	15
1.3.6 Presentation of Numerical Models.....	16
Chapter 2 Literature Review.....	17

2.1. Unified IACS Polar Rules.....	17
2.1.1 Origin of the IACS Polar Rules	17
2.1.2 Load Design Scenario	20
2.2 Ship Ice Contact and Pressure-Area Curves	23
2.2.1 The Ship-Ice Contact Mechanism.....	23
2.2.2 Spatial Pressure Distribution.....	24
2.2.3 Process Distribution	26
2.2.4 Spatial vs. Process.....	27
2.3 Studies using Finite Element Analysis Programs	29
2.3.1 Studies Using DYNA.....	29
2.3.2 Studies using other FEA Programs	31
2.4 Summary of Literature Review.....	32
Chapter 3 Ice Material Model.....	35
3.1 Simulation Setup.....	35
3.1.1 Geometric Model	35
3.1.2 Material Models	38
3.1.3 Element Choices	40
3.1.4 Boundary and Initial Conditions.....	40
3.1.5 Other Inputs	41

3.1.6 Mesh Convergence Study	41
3.1.7 Nominal Contact Area	42
3.2 Ice Material Models Based on the Crushable Foam Material.....	45
3.2.1 Gagnon’s Crushable Foam Ice Model	45
3.2.2 Ice Model A	47
3.2.3 Ice Model B.....	49
3.2.4 Ice Model C.....	51
3.3 Ice Material Models Based on the Elastic-Plastic Material	53
3.3.1 Ice Model D	53
3.3.2 Ice Model E.....	54
3.4 Summary	56
Chapter 4 ALE Method	59
4.1 Simulations for Evaluating the Computation Cost	59
4.1.1 Geometric Model	59
4.1.2 Material Models	62
4.1.3 Element Choices	63
4.1.4 Boundary and Initial Conditions.....	64
4.1.5 Other Inputs	66
4.1.6 Mesh Convergence.....	66

4.1.7 Evaluation of the Computation Cost.....	69
4.2 Oscillatory Analysis vs. Transient Analysis	70
4.2.1 Geometric Model	71
4.2.2 Material Models.....	73
4.2.3 Element Choices	73
4.2.4 Boundary and Initial Conditions.....	73
4.2.5 Loading Conditions.....	75
4.2.6 Added Mass using the Oscillatory Analysis	75
4.2.7 Added Mass using the Transient Analysis	76
4.2.8 Comparison.....	79
4.3 Estimation of Added Mass and Damping Coefficient	80
4.3.1 Geometric Model	80
4.3.2 Material Models	82
4.3.3 Element Choices	82
4.3.4 Boundary and Initial Conditions.....	82
4.3.5 Loading Conditions.....	83
4.3.6 Ship's Added Mass and Damping Terms	84
4.3.7 Ice Added Mass and Damping Terms.....	88
4.3.8 Comparison.....	90

4.4 Summary	91
Chapter 5 Ship Ice Collision Force.....	94
5.1 Defined-Curve-Functions	94
5.1.1 Restoring Forces	94
5.1.2 Implementation	96
5.1.3 Drag and Added Mass.....	100
5.2 Mass Reduction Coefficient.....	101
5.2.1 Simulation Setup.....	102
5.2.2 Results.....	104
5.3 Simulation Setup.....	107
5.3.1 Geometric Model	107
5.3.2 Material Models	107
5.3.3 Element Choices	107
5.3.4 Boundary and initial conditions	107
5.3.5 Loading Conditions and Damping	108
5.3.6 Mesh Convergence.....	108
5.4 Ship-Ice Contact Force	111
5.4.1 “Dry” Collision Cases.....	111
5.4.2 “Wet” Collision Cases	113

5.4.3 “Dry” vs. “Wet”	115
5.5 Summary	119
Chapter 6 Ship’s Structural Response	121
6.1 Ship Structural Design	121
6.1.1 Main Frames	122
6.1.2 Load Carrying Stringers.....	124
6.1.3 Deep Web Frames.....	125
6.1.4 Bulkheads.....	126
6.1.5 Summary	127
6.2 Simulation Setup.....	129
6.2.1 Geometric Model	129
6.2.2 Material Model.....	130
6.2.3 Element Choices	131
6.2.4 Boundary and initial conditions	132
6.2.5 Loading Conditions and Damping.....	132
6.3 Ship Structural Response	133
6.3.1 Contact Force and Pressure.....	133
6.3.2 Von Mises Stress.....	135
6.3.3 Pressure-Deflection Curve	138

6.4 Summary	140
Chapter 7 Conclusions and Recommendations	142
7.1 Conclusions.....	142
7.2 Recommendations.....	143
Chapter 8 Bibliography	148
Appendices.....	156
Appendix A: STePS2 Cluster Specifications.....	157
Appendix B: DYNA's Keyword File of the Final Model.....	159

List of Tables

Table 2-1: Polar Classes in IACS Unified Polar Rules.....	20
Table 2-2: Ice Strength Terms in the URI	22
Table 3-1: Geometry of the Ship and Ice	38
Table 3-2: Material Properties of the Ship Model	38
Table 3-3: Material Properties of the Ice Model.....	39
Table 3-4: Element Choices for Ship and Ice	40
Table 3-5: Surge Distance x and Nominal Contact Area <i>Anominal</i>	44
Table 3-6: Material Properties of Gagnon’s Ice Model	46
Table 3-7: Stress-Strain Relationship in Gagnon’s Ice Model	46
Table 3-8: Material Properties of Ice Model A.....	48
Table 3-9: Stress – Volumetric Strain Relationship in Ice Model A	48
Table 3-10: Stress – Volumetric Strain Relationship in Ice Model B	50
Table 3-11: Stress – Volumetric Strain Relationship in Ice Model C	51
Table 3-12: Material Properties of Ice Model D.....	53
Table 3-13: Material Properties of Ice Model E	55
Table 3-14: Stress – Volumetric Strain Relationship in Ice Model E.....	55
Table 3-15: Summary of Proposed Ice Material Models.....	56
Table 4-1: Element Choices for the ALE Simulations	63
Table 4-2: Summary of the Mesh Convergence Study	68
Table 4-3: Dimensions of the ALE Domain	72
Table 4-4: Influence of the Magnitude of the Force on the Heave Added Mass	77

Table 4-5: Heave Added Mass Coefficients at Very-Low Frequencies and Very-High Frequencies on the Unit Hemisphere	79
Table 4-6: Boundary Conditions on the Ship and Ice	83
Table 4-7: Values of Applied Loads	84
Table 4-8: Added Mass and Damping Terms of the Ship	87
Table 4-9: Added Mass and Damping Terms of the Ice	90
Table 4-10: Added Mass Coefficients Calculated by DDePS (1967) and Present Work ..	91
Table 5-1: Load Definition for Restoring Forces.....	99
Table 5-2: Radii of Gyration Estimated by DYNA and DDePS.....	105
Table 5-3: Mass Reduction Coefficients C_o	106
Table 5-4: Load Definitions on the Ship and Ice	108
Table 5-5: Computation Time of Simulations using Various Element Sizes	109
Table 5-6: Maximum Contact Force (Finite Ice, Dry Collision).....	112
Table 5-7: Maximum Contact Force (Infinite Ice, Dry Collision).....	112
Table 5-8: Maximum Contact Force (Finite Ice, Wet Collision).....	114
Table 5-9: Maximum Contact Force (Infinite Ice, Wet Collision)	114
Table 5-10: Dry vs. Wet – Maximum Contact Force, Finite Ice	116
Table 5-11: Dry vs. Wet – Maximum Contact Force, Infinite Ice.....	116
Table 6-1: Hull Area Extents (IACS 2010)	122
Table 6-2: Scantlings of Structural Members in the Bow Region	128
Table 6-3: Material Parameters for the Non-Rigid Part of the Ship.....	130
Table 6-4: Material Parameters of the Rigid Part of the Ice	130

Table 6-5: Element Choices.....	132
Table 6-6: Load Definition on the Ship.....	133

List of Figures

Figure 1-1: Comparison of Lagrangian, Eulerian and ALE (LSTC, 2010)	10
Figure 1-2: Coupling in the ALE method	12
Figure 1-3: Comparison of SOFT Options	14
Figure 1-4: Contact Model with $SOFT = 2$	15
Figure 2-1: Map of the Arctic Ice-Covered Water Defined by IMO	19
Figure 2-2: Sketch of Ice Contact with a Structure (Daley 2004)	24
Figure 2-3: Spatial Pressure-Area Relationship (Daley 2004).....	25
Figure 2-4: Nominal, true and measured areas (Daley 2004)	25
Figure 2-5: Process Pressure-Area Relationship (Daley 2004)	26
Figure 2-6: Link between Process and Spatial Distributions (Daley 2004).....	28
Figure 3-1: Geometric Models of the Ship and Ice in Rhinoceros®	36
Figure 3-2: the Ice Block with Rounded Edges	36
Figure 3-3: Ship Bow	37
Figure 3-4: Separation between the Ship and Ice (Top View).....	37
Figure 3-5: Stress – Volumetric Strain Curve of the Ice Model in Convergence Study....	39
Figure 3-6: Boundary Condition on the Infinite Ice	41
Figure 3-7: Mesh Convergence.....	42
Figure 3-8: Intersection of the Ship and Ice.....	43
Figure 3-9: Stress-Volumetric Strain Relationship in Gagnon’s Ice Model	46
Figure 3-10: Process Pressure-Area Curve of Gagnon’s Crusable Foam Ice Model.....	47
Figure 3-11: Stress – Volumetric Strain Curve in Ice Model A	48

Figure 3-12: Pressure – Area Curve of Ice Model A	49
Figure 3-13: Stress – Volumetric Strain Curve in Ice Model B	50
Figure 3-14: Pressure – Area Curve of Ice Model B	51
Figure 3-15: Stress – Volumetric Strain Curve of Ice Model C	52
Figure 3-16: Pressure – Area Curve of Ice Model C	52
Figure 3-17: Pressure – Area Curve of Ice Model D	54
Figure 3-18: Pressure – Area Curve of Ice Model E.....	55
Figure 3-19: Pressure - Area Curve of Ice Model C (All Data Included).....	58
Figure 4-1: Top View of the Geometric Model in Rhinoceros®.....	61
Figure 4-2: 3D Model in DYNA.....	62
Figure 4-3: the ALE Domain including Ambient Layers	65
Figure 4-4: Convergence of the Ice Surge Motion	67
Figure 4-5: Convergence of Sway Motion of Ice	67
Figure 4-6: Convergence of the Ice Heave Motion.....	68
Figure 4-7: 3D Model in DYNA.....	72
Figure 4-8: Prescribed Heave Motion of the Sphere in the Oscillatory Analysis.....	74
Figure 4-9: Heave Motion of the Semi-Submerged Sphere.....	76
Figure 4-10: Time History of the Semi-Submerged Sphere’s Heave motion.....	78
Figure 4-11: Influence of the Magnitude of the Force on the Heave Added Mass.....	78
Figure 4-12: 3D Model for Estimating the Added Mass Coefficients on the Ship.....	81
Figure 4-13: 3D Model for Estimating the Added Mass Coefficient on the Ice.....	81
Figure 4-14: Time History of the Ship Heave Motion.....	85

Figure 4-15: Time History of the Ship Roll Motion	86
Figure 4-16: Time History of the Ship Pitch Motion.....	87
Figure 4-17: Time History of the Ice Heave Motion	88
Figure 4-18: Time History of the Ice Roll Motion.....	89
Figure 4-19: Time History of the Ice Pitch Motion	89
Figure 5-1: Creating a Rigid Part.....	98
Figure 5-2: Creating the Local Coordinate System	98
Figure 5-3: Normal Direction of the Contact Surface.....	103
Figure 5-4: Contact Location on the Ice	103
Figure 5-5: Mesh Convergence – Ship Glancing with Finite Ice	110
Figure 5-6: Mesh Convergence – Ship Glancing with Infinite Ice	110
Figure 5-7: Comparison of the Contact Force – Dry vs. Wet (Finite Ice)	118
Figure 5-8: Comparison of the Contact Force – Dry vs Wet (Infinite Ice).....	118
Figure 6-1: Hull Area Extents (IACS 2010)	123
Figure 6-2: Main Frames and the Hull.....	124
Figure 6-3: Load Carrying Stringers and the Hull	125
Figure 6-4: Deep Web Frames and the Hull	126
Figure 6-5: Bulkheads including Stiffeners, and the Hull	127
Figure 6-6: Bow Region with Internal Structural Members	129
Figure 6-7: Rigid and Non-Rigid Ship and Ice	131
Figure 6-8: Comparison of the Contact Force: Rigid Ship vs Non-Rigid Ship	134
Figure 6-9: Time History of the Average Pressure	134

Figure 6-10: A Typical Von Mises Stress Distribution on the Main Frame.....	136
Figure 6-11: A Typical Von Mises Stress Distribution on the Deep Web Frame	136
Figure 6-12: Time History of the Effective Stress	137
Figure 6-13: Time History of the Effective Plastic Strain	137
Figure 6-14: Pressure –Deflection Curve of the Main Frame Member	139

List of Nomenclature or Abbreviations

1D	One Dimensional
2D	Two Dimensional
3D	Three Dimensional
ABS	American Bureau of Shipping classification society
ALE	the Arbitrary-Lagrangian-Eulerian method
CAC	Canadian arctic class
CAD	Computer-aided design
Card	A unit where users give inputs into DYNA
CFD	Computational fluid dynamics
CG	Center of gravity
Computation cost/time	Length of time required for the solver to run the numerical model
Computer Cluster	A collection of networked computers that function as a single computer
DDePS	The software Direct Design for Polar Ships
DOF	Degree of freedom
DNV	Det Norske Veritas classification society
DYNA	Refers to either LS-DYNA or MPP-DYNA interchangeably
FE	Finite element
FEA	Finite element analysis
GL	Germanischer Lloyd classification society

IACS	International Association of Classification Societies
IMO	International Maritime Organization
LSTC	Livermore Software Technology Corporation
LR	Lloyds Register classification society
Part	A collection of elements in DYNA with similar properties
Rhinoceros®	A CAD software developed by McNeel North America
Simulation time	Length of time explicitly simulated within the numerical model
URI	Unified Requirements for Polar Ships published by IACS

List of Appendices

Appendix A: STePS2 Cluster Specifications.....	157
Appendix B: DYNA's Keyword File of the Final Model.....	159

Chapter 1 Introduction

The Arctic region is believed to house one of the world's largest oil and gas resources. A United States Geological Survey estimates that 530 billion barrels of potential petroleum are located beneath this area. The ice-infested sea water and other harsh environmental conditions have been challenging the industry ever since the first operation in the Arctic. However, the increasing demand from the global economy, is driving the oil and gas industry to be more and more active in the Arctic region.

Ships operated in the Arctic area can be divided into two main categories: ice-breaking vessels and ice-strengthened ships. Ice-breaking vessels are used to support other operating units and activities. Their strong hull structures enable them to take on heavy tasks such as ice breaking, maneuvering in ice and ice management. Ice-strengthened ships, whose hulls are relatively weaker than ice-breakers, are designed to withstand possible exposure to a certain level of ice load, depending on their ice class. They have limited ability in breaking ice and maneuvering in ice covered water. Common ice-strengthened ships in the Arctic are vessels such as cargo ships, tankers, and supply ships. Historically, ice classifications governing polar ships are regulated by various classification societies. In 2006, the International Association of Classification Societies (IACS) released a set of documents titled Unified Requirements for Polar Ships (URI) to harmonize different ice classification specifications. More ice-strengthened ships complying with the URI are expected in the near future.

Extensive studies concerning ice-breaking vessels have been carried out to understand the mechanism of the hull breaking ice and the physics of the broken ice acting against the hull. Research and experience on the ice-strengthened vessels are relatively limited. The present thesis is primarily concerned with ice-strengthened ships under the new URI. It presents a study using the state-of-art finite element analysis (FEA) program LS-DYNA to investigate the global motion and local structural response of an ice-strengthened ship under ice impact scenarios.

1.1 Scope and Objectives

This thesis details a procedure for analyzing ship-ice collisions using the commercial FEA program LS-DYNA. The final product is a FEA modeling template to evaluate the global motion, and the global and local structural response of an ice strengthened ship under various ice impact scenarios. This study is composed of four subtopics:

- Develop an ice material model whose pressure-area relationship complies with the URI.
- Estimate the added mass and damping coefficients of the ship and ice using the Arbitrary-Lagrangian-Eulerian (ALE) method.
- Model various ship-ice collision scenarios and compare the results with calculations using the Popov model that is consistent with the URI.
- Combine results from previous subtopics to generate a solution for evaluating a ship's structural response under ice impacts for an ice-strengthened ship.

1.2 Thesis Organization

This thesis contains six chapters. This chapter presents the background, objectives and outline of this thesis, and introduces readers to the commercial finite element analysis program LS-DYNA. Its detailed theory manual (Hallquist, 2006) and user manual (LSTC, 2007a, 2007b) are available online. However, background knowledge of computation time cost, the ALE method, and implementation of the user-defined-curve-functions are briefly presented here to support discussions in later chapters. The use of user-defined-curve-functions is an innovative approach for this application developed in this thesis to simulate the water domain where the ship-ice collision takes place.

Chapter 2 is the literature review. General information on previous work on the URI including a short introduction to design scenarios is presented first, followed by the development of basic knowledge of the mechanisms of ship/structure-ice interaction, the ice pressure-area relationships, and a discussion of existing studies on ship-ice collision using FEA programs including LS-DYNA. A summary of the literature review explains the motivation and methodology for this thesis.

Each of Chapter 3 to Chapter 6 addresses one of the subtopics listed in the previous section. Chapter 3 focuses on developing a proper ice material model that fits the purpose of this thesis. Ice material properties and its failure mechanics are the most important factors in determining the ship-ice contact force. The pressure-area relationship is the most direct indication of ice strength. The pressure-area curve specified in the URI is

considered as the benchmark. Various ice material models are evaluated by simulating a simple ship-ice glancing impact scenario. One ice material model is chosen based on closest compliance with the URI.

Chapter 4 explores the possibility of implementing the ALE method. ALE simulations in LS-DYNA have been successfully implemented to simulate the fluid domain in many studies on ship-ice collision. So naturally it is selected as a tool for this thesis. However, existing studies using ALE are all concerned with the global motion of floating bodies and the global contact forces. This thesis aims at evaluating the ship-ice collision in both the global and local contexts. A discussion in this chapter will show that the ALE method is not an efficient approach due to the high computation cost. An alternative solution featuring user-defined-curve-functions is then proposed and discussed in Chapter 5. Rather than simulating the whole fluid domain, the ALE method is employed to estimate added mass and damping coefficients which can be input into user-defined-curve-functions. Simulations of transient and oscillatory analyses are conducted to estimate those coefficients and results are compared with literature.

Chapter 5 explains modeling the global contact force of a ship-ice collision. The ship is simplified as rigid and the ice is modeled using the material model developed in Chapter 3. Hydrodynamic forces are modeled using user-defined-curve-functions without actually simulating water. Simulations of various ship-ice collision scenarios are performed and

results are compared to calculations using the Popov model which is consistent with the URI.

In Chapter 6, the ship used in previous sections is ice strengthened in accordance with the URI. This structured and deformable ship is then put in the collision models developed in Chapter 5 in lieu of the rigid one. The ship's global motion, and its global and local structural responses under ice impacts are analyzed. The final FEA model can be used as a template for analyzing other ship-ice collision problems.

Chapter 7 concludes the complete study and recommends future work.

1.3 LS-DYNA

The commercial finite element program LS-DYNA is the primary numerical tool for this research. This section introduces readers to its general characteristics, as well as some of its background theories that are relevant to this thesis.

1.3.1 General Information

LS-DYNA is a general-purpose finite element program developed by the Livermore Software Technology Corporation (LSTC) and widely used by the automobile, construction, military, aerospace, manufacturing, and bioengineering industries. Its core-competency is highly nonlinear transient dynamic finite element analysis using explicit time integration. "Transient dynamic" implies the analysis of high-speed, short-duration

events where inertial forces dominate. Ship-ice collision could be a typical transient dynamic problem. “Explicit” means solving equations that involve time and time-dependent variables (velocity, acceleration, and inertial, etc.) to accurately capture the dynamic effects. A “nonlinear” problem is generally characterized by at least one of the following complications:

- Boundary nonlinearity --- Contact between parts or objects changes over time or restraints on parts are time dependent.
- Geometrical nonlinearity --- Large deformations occur, thus requiring new equilibrium equations based on the deforming geometry.
- Material nonlinearity --- Materials do not exhibit ideally elastic behavior and this leads to changes in the stress-strain relationship.

Obviously, a ship-ice collision problem fits in all three criteria of nonlinearity. This makes LS-DYNA the best available tool for this research. The detailed theory manual (Hallquist, 2006) of LS-DYNA is available on LSTC’s website. Some important theories related to this thesis will be presented in the chapter.

This thesis utilizes two versions of LS-DYNA. The first one runs on one or more parallel processors in a single computer. This version is used mainly to run small and simple simulations. Another version is MPP-DYNA, which runs on a computer cluster that works like a super computer by connecting a group of independent computers. The cluster used in this thesis has 128 cores and is very powerful in solving large models that contain

elaborate geometry, very refined mesh, complex material models, longer simulation time, complicated boundary conditions or combinations thereof. This efficiency is achieved via model decomposition that dissects the whole model into parts. There are three decomposing methods (LSTC 2007a): the automatic Recursive Coordinate Bisection (RCB) method, the simple heuristic method (GREEDY), and the manual method. In almost all cases, the RCB is the superior method for its robustness.

MPP-DYNA is the tool for most of the simulations presented in this thesis. Since LS-DYNA and MPP-DYNA essentially share the same theories and codes, they will be both referred as LS-DYNA from Chapter 4 onwards unless otherwise specified.

1.3.2 Time Step Control and Total Time Cost

The goal of this thesis is to produce a practical solution for real world ship-ice collision problems. As part of this, computation cost must be taken into consideration. During the solution, LS-DYNA loops through all the possible elements to update the stress and the right hand side force vector. The new time step is determined by the minimum value of all the critical time steps over all elements. Generally speaking, the ship is analyzed using shell elements while ice, water, and air are modeled using solid elements.

For shell elements, the critical time step can be computed from:

$$\Delta t_c = \frac{L_s}{c} \quad \text{Equation 1-1}$$

where L_s is the characteristic length of a shell element and c is the speed of sound:

$$c = \sqrt{\frac{E}{\rho(1-\nu^2)}} \quad \text{Equation 1-2}$$

where E is the Young's modulus, ρ is the material density and ν is the Poisson's ratio.

The default equation for calculating L_s is:

$$L_s = \frac{(1 + \beta)A_s}{\text{Max}(L_1, L_2, L_3, (1 - \beta)L_4)} \quad \text{Equation 1-3}$$

where L_i is the length of side i of the element, β equals 1 for triangle and 0 for quadrilateral elements, and A_s is the surface area of the element.

The critical time step for solid elements is computed in a similar manner:

$$\Delta t_e = \frac{L_e}{Q + (Q^2 + c^2)^{1/2}} \quad \text{Equation 1-4}$$

where L_e is characteristic length, Q is a function of bulk viscosity and c is the adiabatic speed of sound. Equations for calculating Q and c are very complicated and unnecessary to be presented here.

As shown in the equations above, element sizes and material properties together determine the critical time step. Note that in LS-DYNA, rigid elements are not considered in the computation of time step. Users should define a proper time step value when the model only contains rigid elements.

Besides the critical time step, the total computation cost also depends on the number of elements, boundary conditions, and the analysis method. More DOF, more complicated

loading conditions, and the ALE analysis generally require longer computation time. This is a major consideration in this thesis and is further discussed in Chapter 4.

1.3.3 The Arbitrary Lagrangian-Eulerian (ALE) Method

The ALE method is currently the only method for simulating water in DYNA. It has been used in several studies. Its full detailed theory can be found in DYNA's theory manual (Hallquist, 2006). This section only introduces readers to the basic knowledge of the ALE method. Implementation is discussed in Chapter 4.

Figure 1-1 illustrates the difference of the Lagrangian, Eulerian, and the ALE method in analyzing a solid piece of material (red) moving and deforming. In the Lagrangian simulation, the mesh deforms with the material. In the Eulerian solution, the material flows through the fixed mesh. The ALE method is a combination of these two. The mesh is attached to the material (Lagrangian) and passes through the fixed background reference mesh (Eulerian). In other words, the material deforms in a Lagrangian formulation at the first step. The second step is the advection, which means that element state variables in the deformed elements (red ones in Figure 1-1) are remapped back onto the Eulerian reference mesh.

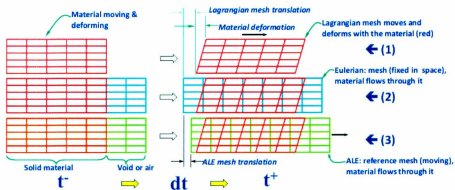


Figure 1-1: Comparison of Lagrangian, Eulerian and ALE (LSTC, 2010)

Fluid-structure interaction analysis using the ALE method requires three additional computations besides the Lagrangian step. The first one is the advection mentioned earlier. It controls the flowing or fluxing of materials in the total ALE domain. The second calculation is interface reconstruction which defines multi-material co-existence in one element. The last one is the coupling between Lagrangian elements and ALE parts (fluid-structure in this thesis). Setup of advection and interface reconstruction is very standard and straightforward in the ALE simulations, while coupling requires user's defined inputs. Note that the element size of Lagrangian parts should be similar to that of the ALE parts for the ALE algorithm to function accurately.

The coupling calculation in the ALE method is penalty based and is demonstrated in Figure 1-2. In the left part of Figure 1-2, there is no coupling force since the shell structure (green) is not in contact with the water (Eulerian material in red). Once penetration occurs, it is measured to compute the coupling force as a spring system. The

spring stiffness depends on the material properties of all bodies involved. The penalty factor named PFAC, a scale factor of scaling the estimated stiffness is required for calculating the coupling force. This PFAC, whose default value is 0.1, is recommended to be redefined by the user. Its value can be either a constant or a function of penetrating depth. Note that its value is different in each analysis. Even in the same analysis, if the element size or the geometric model is modified, its value needs to be re-calibrated. Prior to conducting a detailed ALE simulation, several experimental simulations are generally needed to determine a proper value. In each ALE simulation presented in this thesis, the PFAC is set to a value so that the floating body's neutral buoyancy in the simulation is the same as that determined by a simple hydrostatic calculation based on its geometry. However, the floating body still oscillates around the neutral position with very small amplitude. It is almost impossible to determine the optimal PFAC value to completely eliminate this small oscillation. Many hours were spent on calibrating the PFAC value during this research to minimize the noise it may introduce to the solution.

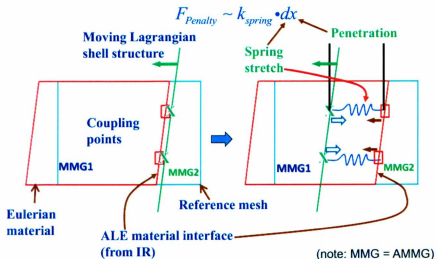


Figure 1-2: Coupling in the ALE method

1.3.4 Contact Model

There are two types of contact algorithms in LS-DYNA. The first one is “one-way contact”. It only checks the user-specified slave nodes for penetration of the master segments. It then transfers compression loads between the slave nodes and the master segments. When contact friction is active, tangential loads are also transmitted if relative sliding happens. A Coulomb friction formulation is used with an exponential interpolation function to transition from static to dynamic friction. This transition requires a decay coefficient. It only works when the static friction coefficient is larger than the dynamic friction coefficient. One-way contacts may be appropriate when the master part is rigid. It may also be used for deformable bodies when the master part has a coarse mesh and the

slave part has a relatively fine mesh. Other common applications are contacts of beam-to-surface or shell-edge-to-surface.

The other type is the “two-way contact”. It functions essentially in the same way as the “one-way contact”, except that the subroutines checking the slaves nodes for penetration are called a second time to check the master nodes for penetration through the slave segments. In other words, the treatment is symmetric and the definition of the slave surface and master surface is arbitrary. This method results in higher computation cost due to the extra subroutine calls.

The automatic-single-surface-contact is a “two-way contact” and is recommended as the superior algorithm by DYNA. The soft constraint option (SOFT) can be added into the contact stiffness calculation by the user. When SOFT is set at 1, the contact algorithm adopts the soft constraint formulation. It is effective for contacts involving dissimilar mesh sizes and dissimilar material properties. The pinball segment based contact is activated by setting SOFT at 2. It is the recommended option for treating contact at sharp corners. Simulations of a ship impacting an ice block with rounded edges were carried out to examine their difference. The ship and ice had dramatically different material properties. In each simulation, a different SOFT option is chosen. Resultant contact forces are compared in Figure 1-3. Time histories of the contact forces using different SOFT options are similar to each other and roughly have the same peak value. Measuring the distance between the ship and ice indicates that the contact should starts at about 1.1

seconds. In all simulations, DYNA detects a contact before the bodies are actually in contact. This is marked as the vertical line (purple) in the figure. However, in the case where $SOFT = 2$, the contact occurs much earlier than other cases. Figure 1-4 is a snapshot from the simulation where $SOFT = 2$. The ship is in red and the ice block is in blue. It shows that the ice (blue) is already deformed before the geometries are in contact. This phenomenon also exists in the case where $SOFT = 1$, but is much less severe. This “early contact” affects the analysis of the nominal contact area and hence the ice pressure-area relationship. It is discussed in Chapter 3. The automatic-single-surface-contact is used for all simulations in this study. The value of $SOFT$ is set at 1 in almost all simulations.

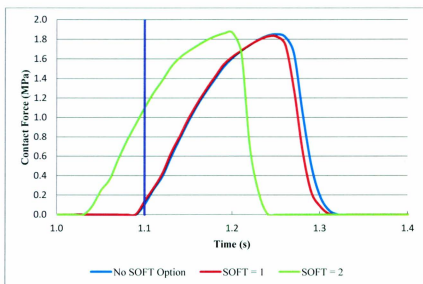


Figure 1-3: Comparison of SOFT Options

Note: The vertical purple line marks the time instant when the contact should initiate.

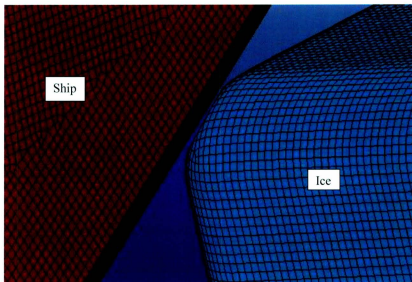


Figure 1-4: Contact Model with SOFT = 2

1.3.5 User Defined Curve Function

In DYNA, the *DEFINE_CURVE_FUNCTION card defines a curve where the abscissa is time, and the ordinate is expressed by a function of other curve definition, forces, kinematical quantities, intrinsic functions, interpolating polynomials, and combinations thereof. For instance, the displacement curve function reports the displacement (ordinate) over the time (abscissa). Then an external load can be defined as the displacement multiplied by a coefficient. A full list of the *DEFINE_CURVE_FUNCTION is available in DYNA's Keyword User's Manual (2007). Functions that give values of z-translational displacement (heave), y-rotational displacement (pitch), and x-rotational displacement (roll) are used in this thesis. Detailed implementation is addressed in Chapter 5.

1.3.6 Presentation of Numerical Models

A numerical model is constructed in DYNA by entering inputs in “cards”, each of which is for a specific purpose. When a simulation is presented, only important inputs is selected and organized into the following categories:

- Geometric model: This category gives the detailed information on the dimensions of the geometric model. Geometric models can be generated in DYNA or other CAD programs. Rhinoceros® (McNeel North America) is used in this thesis for producing geometric models.
- Material models: This section discusses material types and their parameters.
- Element choices: This category presents choices of element types (solids, shells, etc.) as well as element parameters such as the shell thickness, element formulations, ambient types, and integration algorithms.
- Boundary conditions and initial conditions: In DYNA, the boundary conditions define the confinement on objects and their prescribed motions. The initial conditions include initial velocities, initial strains, the initial hydrostatic pressure distribution, and the initial volume fraction, etc.
- Other settings: The section covers the load definition, the contact model, damping definition, user defined functions, etc.
- Mesh convergence: The appropriate element size is determined via the mesh convergence study.
- Results declaration: This part presents and discusses the results.

Chapter 2 Literature Review

Studies on icebreaking vessels are mostly concerned with the level ice failure mechanism, the global ice resistance on the ship, and the movement of broken ice floes around the hull. These topics are not covered in this literature review. This literature review examines the topics of ship impacting ice floes, bergy bits, and icebergs. The review focuses on a few areas: origin and theories in the URI, mechanisms of the ship-ice contact, ice pressure-area relationships, and the finite element analysis of ship-ice interaction. Special attention is devoted to studies using DYNA since it is the primary tool for the present thesis. Each topic will be discussed in a separate section followed by a brief summary.

2.1. Unified IACS Polar Rules

This section presents the origin of the URI and a discussion of design scenario which is important to the finite element modeling in later chapters.

2.1.1 Origin of the IACS Polar Rules

There are several major polar ship classifications developed by various countries to protect their arctic waters and interests. They are:

- Canadian ASPPR/CAC (9 Classes)
- Russian MRS/NSR (9 Classes, 4 Icebreaker)
- Finnish/Swedish (Baltic) (5 Classes)
- ABS (USCG) (5 Polar Classes, 5 Baltic Classes)

- DNV (3 Icebreaker, 3 Polar, 5 Baltic Classes)
- LR (5 Polar, 5 Baltic Classes)

A “class” refers to the ice class assigned to a ship by a classification society. Each ice class will have its own requirements regarding hull thickness, structural scantlings, rudders, propellers, mechanical systems, and heating systems.

In recent years, the increasingly globalized industry has demanded a harmonized set of classifications for ships operating in the Arctic waters (see Figure 2-1). In 2006, IACS released a set of Unified Requirement for Polar Class Ships (URI) to complement the Guidelines for Ships Operating in Arctic Ice Covered Waters published by the IMO. The IMO classifications provide a framework for the design and operation of polar ships and the IACS gives specific requirements on structures and machinery. Table 2-1 lists a general description of IACS polar classes. Background theories of the URI can be found in Daley (1999, 2000, 2002), Kendrick et al. (2000a, 2000b, 2009).



Figure 2-1: Map of the Arctic Ice-Covered Water Defined by IMO

Table 2-1: Polar Classes in IACS Unified Polar Rules

Polar Class	Ice Description (based on WMO Sea ice Nomenclature)
PC 1	Year-round operation in all Polar waters
PC 2	Year-round operation in moderate multi-year ice conditions
PC 3	Year-round operation in second-year ice which may include multi-year ice inclusions
PC 4	Year-round operation in thick first-year ice which may include old ice inclusions
PC 5	Year-round operation in medium first-year ice which may include old ice inclusions
PC 6	Summer/autumn operation in medium first-year ice which may include old ice inclusions
PC 7	Summer/autumn operation in thin first-year ice which may include old ice inclusions

2.1.2 Load Design Scenario

The energy method (Popov et al., 1967) solves the maximum ship-ice contact force by equating the normal kinetic energy with the ice crushing energy. A further developed version using the process pressure-area ice crushing model can be found in Daley (1999, 2000, 2001, 2002), and Kendrick et. al, (2000b), and is adopted in the URI. The balance of effective kinetic energy KE_e and the ice crushing energy IE is expressed as (Daley, 1999, and Kendrick et. al, 2000b):

$$KE_2 = IE \quad \text{Equation 2-1}$$

where

$$KE_e = \frac{M_e}{2} V_n^2 \quad \text{Equation 2-2}$$

Where V_n is the normal velocity and M_e is the effective mass and is given as:

$$M_e = \frac{M}{C_o} \quad \text{Equation 2-3}$$

where C_o is the mass reduction coefficient. Its detailed derivation can be found in Popov et al. (1967). It will be discussed in Section 5.3.

This approach rationally links the ice load to the design scenario of an angular ice edge (the edge of a floe or a channel) glancing the shoulder of the bow. The ship is assumed to surge forward at the design speed, hit and penetrate the ice, and then rebound away. The ice crushing force must be smaller than the minimum bending force causing ice flexural failure. Class dependent factors such as ice thickness, ice strength, ship speed, and the bow shape are all included in the derivation. The normal contact force F_n at bow is given as:

$$F_n = \left\{ P_o \left[\frac{\tan\left(\frac{\phi}{2}\right)}{\sin(\beta') \cos(\beta')^2} \right]^{1+ex} \right\}^{\frac{1}{3+2ex}} \left[\frac{1}{2} M_e V_n^2 (3 + 2ex) \right]^{\frac{2+2ex}{3+2ex}} \quad \text{Equation 2-4}$$

where ϕ , β' are the ice wedge angle and normal hull frame angle respectively. The P_o and ex are from the process ice pressure-area relationship:

$$P = P_o A^{ex} \quad \text{Equation 2-5}$$

where P is the total pressure, A is the nominal contact area, P_o is the ice strength term corresponding to the pressure on $1m^2$ nominal loading area. ex is the exponential term which varies over different process pressure-area relationships. In the URI, ex is specified as -0.1 and P_o is class dependent (see Table 2-2). Their values are carefully chosen to ensure that resulting local loads are compatible with both the Western and Russian approaches. The pressure-area relationship in the URI is given in Equation 2-6. The concept of pressure-area curve is explained in the next section.

$$P = P_o A^{-0.1} \quad \text{Equation 2-6}$$

Table 2-2: Ice Strength Terms in the URI

Ice Class	PC 1	PC 2	PC 3	PC 4	PC 5	PC 6	PC 7
$P_o(MPa)$	6.00	4.20	3.20	2.45	2.00	1.40	1.25

Ice loads on non-bow areas (bow-intermediate, mid, stern, and bottom) are converted from the load on the bow by multiplying empirical area factors. The design load is considered as the average pressure over a rectangular load patch. It is statically applied to the ship structure to determine the minimum scantlings. A complete derivation of the design load and framing design is given by Daley (1999, 2000), Daley et al. (2009a, 2009b, 2010), and Kendrick et al. (2000a, 2000b, 2009).

2.2 Ship Ice Contact and Pressure-Area Curves

2.2.1 The Ship-Ice Contact Mechanism

In the earliest ice load models, the total contact force was the primary concern. It was usually estimated with an assumption of uniform pressure distribution within the contact region. After 1980, more field trials and measurements with evolving technologies suggested that the pressures actually vary over many orders of magnitude within the contact region. This mechanism is idealized in Figure 2-2 (Daley 2004). Extruded rubble, spalls, internal cracks, and extrusion can be observed in all ice-structure contact scenarios. Flexural cracks may not be present unless flexural failure takes place. Direct solid contact will exert the highest pressure on the structure and damage the ice. However, the confinement in the direct contact region makes it capable of sustaining very high pressures. Extruded rubble and crushed ice will result in very low pressure at the edge of the contact region. This effect can be represented using a pressure-area plot where the area is the independent variable. Ice strength, thickness, and velocity generally vary in a much smaller range than contact area and have less influence on pressure. Nowadays, the pressure-area relationship has become the most popular presentation of ice pressure data. It is also used to determine both global and local ice loads on structures and ships. There are two distinct types of pressure-area relationships (Frederking 1998, 1999; Daley 1985, 2004, 2007): the process pressure-area relationship and the spatial pressure-area relationship.

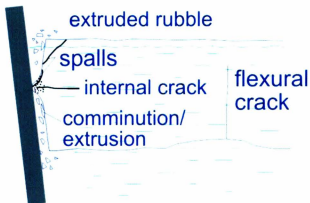


Figure 2-2: Sketch of Ice Contact with a Structure (Daley 2004)

2.2.2 Spatial Pressure Distribution

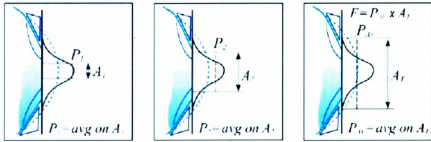
Figure 2-3 explains the spatial pressure distribution which describes the variation of local peak pressure on local areas within a global contact area. At any instant time t of an ice contact event, a very small area A_1 and its corresponding peak local average pressure P_1 can be plotted as the point (A_1, P_1) . A larger area A_2 will necessarily result in a smaller average pressure P_2 . So another point (A_2, P_2) can be located on the plot. Similarly, the average pressure P_t of the whole contact area A_t can be plotted as the point (A_t, P_t) . The spatial pressure-area curve is useful in determining the design load on local structures. It can be expressed as:

$$P = CA^{-e} \quad \text{Equation 2-7}$$

where C varies from 0.5 to 5MPa and e varies from -0.7 to -0.25 in most cases. Note that the area discussed here is the nominal contact area. There are two other area terms: true area and measured area. Their difference is demonstrated in Figure 2-4.

Local distribution of pressure (ideal)

all at time $-t$



Spatial
Pressure Area Plot

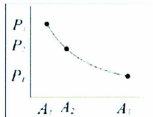


Figure 2-3: Spatial Pressure-Area Relationship (Daley 2004)

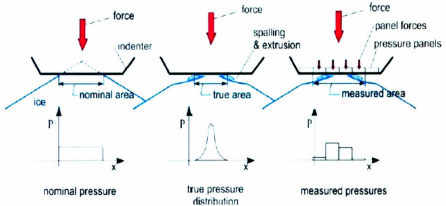


Figure 2-4: Nominal, true and measured areas (Daley 2004)

2.2.3 Process Distribution

The process pressure-area is often used to determine the contact force. It gives the relationship of the average pressure and the total contact area (see Figure 2-5). At the instant time t_1 , the total contact area A_1 , and its corresponding average pressure P_1 can be plotted as the point (A_1, P_1) . As the contact event progresses to the instant time t_2 , the average pressure P_2 over the total contact area A_2 can be plotted as the point (A_2, P_2) . Similarly, at the instant time t_N , the point (A_N, P_N) can be plotted. In this thesis, the discussion of the process pressure-area curve is based on the nominal contact area.

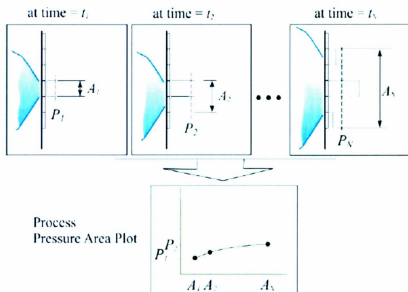


Figure 2-5: Process Pressure-Area Relationship (Daley 2004)

2.2.4 Spatial vs. Process

Figure 2-6 shows the connection between the process and the spatial pressure-area curves. Basically, at any instant time of a contact event, there is a complete spatial pressure-area curve but only one point on the process-area curve. As the impact event develops, there will be a set of spatial pressure-area curves. Joining the ends of them will generate a complete process pressure-area curve of the contact event. The connection of the two indicates that greater total contact area and total contact forces tend to yield higher pressures. The spatial curve inevitably has a trend of falling, while the process curve may rise or fall as the total area increases (Daley 2004, Frederking 1998).

Both spatial and process curves are concepts in the context of a single ice contact event. Most existing pressure-area analyses are based on an assemblage of data and measurements of multiple events therefore cannot be simply categorized as either spatial or process relationships. Those relationships are generally presented in the form:

$$P = kA^n \quad \text{Equation 2-8}$$

where k is the pressure over 1m^2 loading area; A is the loaded area and n is a constant less than 1 (Masterson et al 2007). For example, the pressure-area curve in CSA S471 and API RP 2N is $P = 8.1A^{-0.5}$ (derived by Masterson and Frederking 1993). A few other relationships in this form can be found in Masterson et al. (2007). The pressure-area curve specified by the URI is a process distribution. It is in the form of $P = P_o A^{-0.1}$ as mentioned earlier (see Equation 2-6 and Table 2-2)

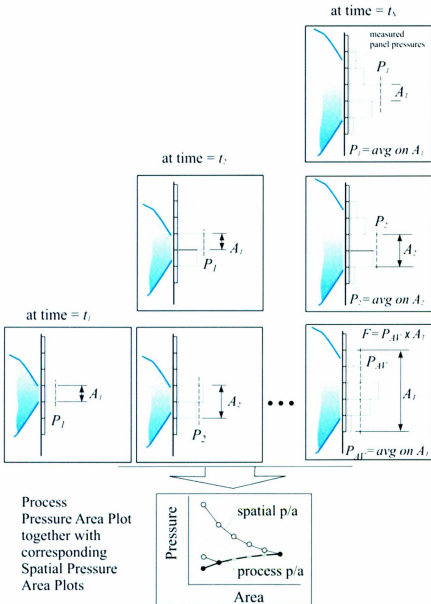


Figure 2-6: Link between Process and Spatial Distributions (Daley 2004)

As stated earlier, the goal of this thesis is to investigate ice-strengthened ships regulated by the URI. Therefore, developing an ice material model whose pressure-area relationship complies with the URI has the utmost importance. It is the cornerstone of this study and is addressed in Chapter 3.

2.3 Studies using Finite Element Analysis Programs

This section reviews studies of the ship-ice interaction problem using finite element analysis. A sub-section is dedicated to studies using LS-DYNA since it is the primary tool for this research. It includes studies using the ALE method. In addition, a few studies using other FEA programs will be presented as well.

2.3.1 Studies Using DYNA

Gagnon et al. (2004) published a paper on a series of model tests of a transiting tanker passing by floating ice floes. Gagnon et al. (2006) reported an ALE simulation of one of the model tests. The numerical solution showed good agreement with the physical test in terms of sway motion. In the same paper, Gagnon proposed a crushable foam material model for simulating ship colliding with a bergy bit in DYNA. This innovative material model was validated against data from actual measurements. Note that all simulations in this study only allowed the ship to move forward and restrained it in all other DOF.

Wang et al. (2010a) proposed a study of ice resistance on the Canadian icebreaker Terry Fox in level ice. The ice failure envelop developed by Derradji-Aouat (2003) was adopted

and modified to model level ice. The fluid domain was modeled using the ALE method. The ship was fixed in all DOF except the surge motion. Simulations including water, and not including water, were compared with full-scale measurements. Water was proven important in numerical analysis of ship breaking level ice.

Wang et al. (2010b) further investigated modeling fluid structural interaction using DYNA. A wave maker was simulated using the ALE method. The wave length and wave height from the numerical simulation were in reasonable agreement with the experimental results. An ALE simulation of a thin ice piece floating in water was also performed, and showed good results of the buoyancy force on the ice and its vertical displacement. Later in the paper, simulations of the Terry Fox moving through water covered by ice pieces were conducted and global ice forces on the ship were recorded. In the study, the ship was modeled as a rigid body and free to move only in the surge direction. Ice pieces were treated as rigid bodies with uniform shape and size. Mesh dependency was not investigated.

Extra attention was devoted to reviewing literature on ship local structural response under ice loads using DYNA. Unfortunately, only a few studies were found. The first one was the Master's thesis by Myhre (2010) at the Norwegian University of Science and Technology. In his analysis of an ice collision with a section of the mid-ship structure, the part of the ice that could possibly be affected by the contact was modeled using the ice model developed by Liu et al. (2009). This is a material model based on the Tsai-Wu

failure criterion. The rest of the half spherical ice was treated as rigid to save computation cost. This was a very efficient approach. Liu's ice model is discussed in the next subsection.

The other two studies using DYNA were very similar to each other. Lee et al. (2007) explored the possibility of global 2D modeling of ship-ice interaction using DYNA. The ship-ice contact force was determined via a global analysis, and then a section of LNG side structure was analyzed in a local FEA. Kim et al. (2011) followed the similar approach. They first estimated the load by global analysis, and then applied it to a section of a cargo ship to determine the local structural strength.

2.3.2 Studies using other FEA Programs

Kwak et al. (2006) analyzed a section of the bow structure of an Arctic tanker under ice loads. Ice models with different elastic modulus, failure stresses, and yield stresses were tested in simulations of collision between the rigid bow and deformable ice. One ice model gave the contact force that complies with the URI. Then this ice model was used to collide with the flexible bow to evaluate the ship structural strength. Water and hydrodynamic effects were not included in the analysis. The methodology of adjusting ice material properties in this study is useful to the present work.

Wang et al. (2008a) evaluated the structural integrity of an LNG ship under a ship-ice collision. They used a combination of global and local finite element analysis modeling.

The global simulation treated the ship as elastic-plastic and ice as crushable foam with a material failure criterion. It estimated the ship-ice contact force, contact area, material deformation, and material failure. In the local finite element analysis model, the ice load was applied statically to a section of the mid-ship structure to determine the critical load. This work defined a procedure for evaluating hull structure in LNG ships under ice loads.

Following this procedure, Wang et al. (2008b) investigated another cargo ship's structural response under ice impact. Different from their previous work, they adopted the URI to determine the values of ice load and loading area rather than a global simulation. The ice patch loads from six different collision scenarios were then applied to a local model of the mid-ship to assess its strength.

Liu et al. (2009) proposed an ice material model based on the Tsai-Wu failure criterion, which associates damage with plastic strain, for analyzing a collision between a bergy bit and a section of mid-ship structure. The pressure-area curve $P = 7.4A^{-0.7}$ defined by ISO (2008) was the benchmark for Liu's ice model. Compared to the pressure-area relationship specified in the URI, Liu's solution overestimated pressure when the contact area was small, i.e., a ship impacting a small ice floe.

2.4 Summary of Literature Review

A few conclusions can be drawn from the literature review. There is a need for an ice material model that is shown to comply with the URI for ship-ice collision analyses using

DYNA. It is necessary to verify if the crushable foam model (Gagnon et al. 2006) could be used in this study. If not, developing a suitable ice model will be a priority.

Existing finite element solutions for ship-ice collision problems can be categorized as follows:

- Modeling ice impacting a section of the ship structure: Kwak et al. (2006), and Myhre (2010).
- Modeling the local ship structure under static ice loads rather than simulating the impact: Wang et al. (2008b)
- Using a simplified global ship-ice collision model to determine the contact force and then applying that force statically to the ship structure in a separate analysis of the local ship structure: Wang et al. (2008a), Lee et al. (2007), Kim et al. (2011).
- Analyzing ship-ice contact using global modeling where hydrodynamics is included but the ship structural response is not: Wang et al. (2010a) and Wang et al. (2010b).

Each of their methods has pros and cons. The first type does not include global motion or hydrodynamic forces. The second one does not consider global motion, hydrodynamic forces, ice strength, or the dynamic effect of ice load. However, both of them are very quick solutions. The third one is more comprehensive than the previous two but the procedure is complicated. Conducting two separate analyses could be time consuming.

Although the last category is the only one that models hydrodynamic effects, it is only concerned with the global contact and motion. It may not be a cost-effective solution once the ship structural response is involved. An ideal solution would combine hydrodynamic forces, the global motions of the ship and ice, the contact force, ice failure, and the ship structural response in one efficient analysis. This is the goal of the present thesis.

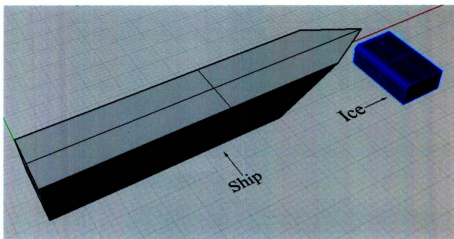


Figure 3-1: Geometric Models of the Ship and Ice in Rhinoceros®

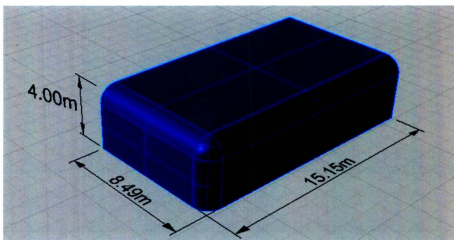


Figure 3-2: the Ice Block with Rounded Edges

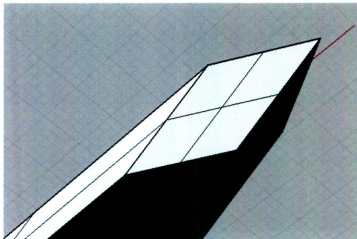


Figure 3-3: Ship Bow

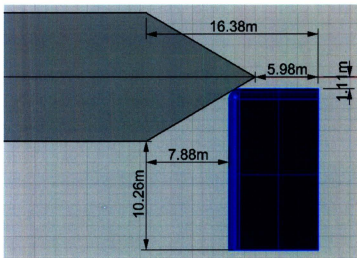


Figure 3-4: Separation between the Ship and Ice (Top View)

Table 3-1: Geometry of the Ship and Ice

	Ship	Ice
Overall Length	66.0m	8.494m
Length at Waterline	61.8m	8.494m
Beam	12.0m	15.154m
Height	7.20m	4.00m
Draft	4.80m	3.510m
Corner Radius	N/A	1.0m
Waterline Angle α	30°	N/A
Sheer Angle γ	60°	N/A
Frame Angle β	45°	N/A
Waterplane Coefficient	0.75	1.0
Block Coefficient	0.79	1.0

3.1.2 Material Models

The ship is always treated as a rigid body for the work covered in this chapter. Its material properties are listed in Table 3-2.

Table 3-2: Material Properties of the Ship Model

Card ID	MAT_RIGID (MAT_020)		
Material Type	Density	Young's Modulus	Poisson's Ratio
Rigid	7850kg/m ³	207GPa	0.3

Each simulation investigated a different ice material model. Those that showed the best results are presented in this chapter. An ice model based on the crushable foam material is used in the mesh convergence study. Its parameters and the stress-strain relationship are shown in Table 3-3 and Figure 3-5. Those parameters have minor influence on the mesh convergence.

Table 3-3: Material Properties of the Ice Model

Card ID	MAT_CRUSHALBE_FOAM (MAT_063)			
Material Type	Density	E	Poisson's Ratio	Tensile Stress Cutoff
Elastic-Plastic	$900\text{kg}/\text{m}^3$	9GPa	0.003	800MPa

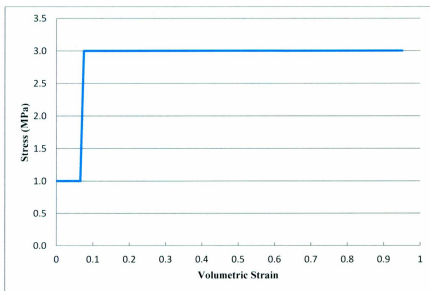


Figure 3-5: Stress – Volumetric Strain Curve of the Ice Model in Convergence Study

3.1.3 Element Choices

Automatic meshing is used to create the ship and ice mesh models. The rigid ship is meshed using shell elements and the ice block is meshed with solid elements. Information on the element formulation and element type are listed in Table 3-4. The fully integrated formulation is a very fast algorithm and it is chosen for the rigid shell elements. If shell elements are used to mesh a non-rigid body, the Belytschko-Tsay formulation will be the best choice. It is the recommended option for most structural analysis (Quinton, 2009). The default solid element (1 point solid) is chosen for ice for its superior robustness. Other fully-integrated solids are less stable when the deformation is large because one of the integration points may have a negative jacobian while the whole element maintains a positive volume. The convergence study that determines the proper element size is presented in Section 3.1.6.

Table 3-4: Element Choices for Ship and Ice

Part	Element Type	Formulation Option	Ambient Type
Ship	Shell	16 (Fully Integrated)	N/A
Ice	Solid	1 (Default)	0

3.1.4 Boundary and Initial Conditions

In each simulation, two faces of the ice block are fixed (see Figure 3-6). The ship is free to move in the longitudinal direction, but confined in all other 5 DOF. It starts moving forward towards the ice at an initial speed of 3m/s. After moving for about 4.02m, the ship bow begins impacting the ice block at the rounded corner. The ice is then gradually

crushed and deforming as the collision proceeds. At the same time, the ship slows down until the end of the simulation.

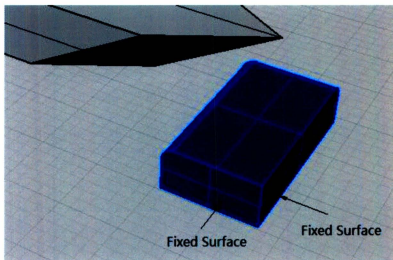


Figure 3-6: Boundary Condition on the Infinite Ice

3.1.5 Other Inputs

The recommended automatic-single-surface-contact is used. As discussed in Section 1.3.4, its SOFT option is set at 1 since the material properties of the ship and ice are dramatically different. There is no gravity or any other external load. No damping is added to the system.

3.1.6 Mesh Convergence Study

A mesh convergence study is conducted by comparing the time histories of the contact forces. Figure 3-7 shows that convergence is reached when the element size is smaller

than 0.35m. For subsequent simulations, 0.24m is then considered as an appropriate element size for subsequent simulations.

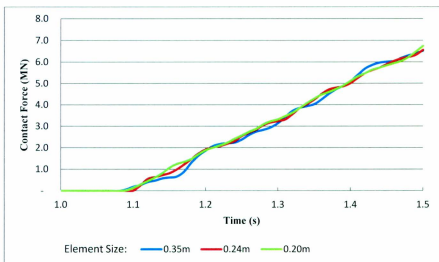


Figure 3-7: Mesh Convergence

3.1.7 Nominal Contact Area

After each simulation is completed, the time history of the contact force is directly obtained from the simulation's outputs. The time history of the nominal contact area could not be accurately given by DYNA due to the coarse mesh, so it is derived using the CAD program Rhinoceros®. The procedure can be illustrated in Figure 3-8. After the ship is moved forward for a distance x from its initial position A to the new location B , an intersection of the ship and ice can be created as the yellow curve. The surface area of the yellow curve is considered as the nominal contact area corresponding to the surge distance x .

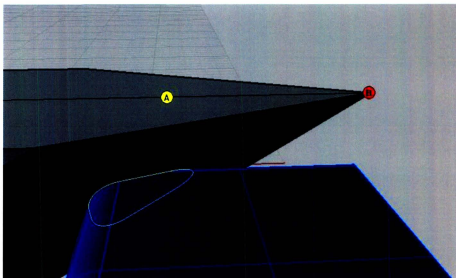


Figure 3-8: Intersection of the Ship and Ice

Values of the ship surge distances and corresponding nominal contact areas are listed in Table 3-5. The relationship between x and $A_{nominal}$, as obtained by the line of best fit, is shown in Equation 3-1. It is applicable for all simulations presented in this chapter. In each simulation, the time history of the ship surge distance is provided by DYNA. It is then substituted into Equation 3-1 to yield the time history of the nominal contact area for that simulation. The process pressure-area curve of the ice is then generated by analyzing the time history of the contact force and the time history of the nominal contact area

Table 3-5: Surge Distance x and Nominal Contact Area $A_{nominal}$

$x(m)$	$A_{nominal}$	$x(m)$	$A_{nominal}$
4.530	0.000	4.999	1.045
4.549	0.042	5.000	1.048
4.569	0.089	5.500	2.200
4.609	0.182	6.000	3.541
4.649	0.273	6.500	5.101
4.709	0.408	7.000	6.881
4.749	0.496	7.500	8.882
4.789	0.583	8.000	11.103
4.849	0.715	8.500	13.545
4.889	0.802	9.000	16.207
4.939	0.913	9.500	19.089
4.969	0.979	10.000	22.193

$$A_{nominal} = \begin{cases} 0, & x < 4.53 \\ 2.2207x - 10.054, & 4.53 < x < 5 \\ 0.0016x^3 + 0.4014x^2 - 2.0801x + 1.2171, & x \geq 5 \end{cases} \quad \text{Equation 3-1}$$

Recall the discussion in Section 1.3.4 and Figure 1-4, which show that DYNA detects a contact before the geometries are actually in contact. This phenomenon means that the nominal contact area derived in Rhinoceros® is different from that in DYNA. Although setting SOFT =1 helps minimize this discrepancy, it still makes the analysis of the

pressure-area relationship less accurate, especially when the contact area is small.

Therefore, analysis in this chapter does not include data from contacts where the nominal contact area is less than $0.4m^2$.

3.2 Ice Material Models Based on the Crushable Foam Material

This section presents the results of modeling ice using the crushable foam material model available in DYNA. Different models are developed by changing the parameters in the crushable foam model. More than 30 models were evaluated and several of them have showed the desired results. In addition, a previous model (Gagnon et al. 2006) is introduced in this section.

3.2.1 Gagnon's Crushable Foam Ice Model

Gagnon's ice model (Gagnon et al. 2006) was initially developed to reproduce the spatial pressure-area curve with a high central peak load. It is necessary to determine if it fits the purposes of this study. Gagnon's model is based on the crushable foam material model where the deformation is mostly unrecoverable. Its key parameters are listed in Table 3-6. The small Poisson's ratio limits the material's deformation in directions other than the loading direction. The relationship of stress and volumetric strain is shown in Table 3-6 and Figure 3-9. Note that in the crushable foam material model, the material's behavior follows the stress-strain relationship rather than the Young's modulus.

Table 3-6: Material Properties of Gagnon's Ice Model

Card ID	MAT_CRUSHALBE_FOAM (MAT_063)		
Density	Young's Modulus	Poisson's Ratio	Tensile Stress Cutoff
900kg/m^3	9GPa	0.003	8MPa

Table 3-7: Stress-Strain Relationship in Gagnon's Ice Model

Stress (MPa)	0.1	0.1	50.0	50.0
Volumetric Strain	0.000	0.065	0.075	0.890

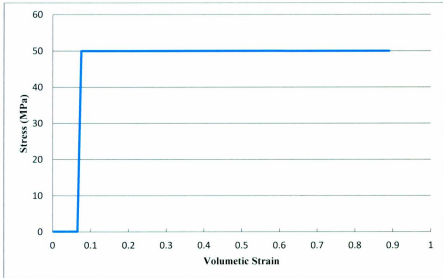


Figure 3-9: Stress-Volumetric Strain Relationship in Gagnon's Ice Model

A process pressure-area curve of Gagnon's ice model is shown in Figure 3-10. This curve does not fit the form of $P = P_0 A^{-0.1}$. In later sections the properties are modified to develop models with the desired pressure-area relationship to serve the purposes of this study.

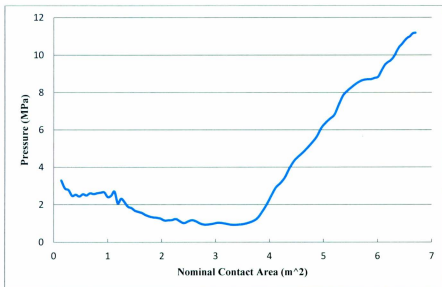


Figure 3-10: Process Pressure-Area Curve of Gagnon's Crusable Foam Ice Model

3.2.2 Ice Model A

The tensile stress cutoff (TSC) value in Gagnon's model is $8MPa$. Ice models with significantly different TSC values were tried and they all displayed unsuitable behavior. The Young's Modulus has a minor impact on the pressure-area curve as long as its value is in the realistic range. The stress-volumetric strain relationship is the dominant factor in the form of the pressure-area curve. Material density and Poisson's ratio are not altered.

Table 3-9 and Figure 3-11 shows the redefined stress-strain relationship in the modified crushable foam ice model-A. Other parameters are listed in Table 3-8.

Table 3-8: Material Properties of Ice Model A

Card ID	MAT_CRUSHALBE_FOAM (MAT_063)		
Density	Young's Modulus	Poisson's Ratio	Tensile Stress Cutoff
900kg/m^3	5GPa	0.003	8.00MPa

Table 3-9: Stress – Volumetric Strain Relationship in Ice Model A

Volumetric Strain	0.000	0.065	0.075	0.900
Stress (MPa)	2.0	2.0	6.0	6.0

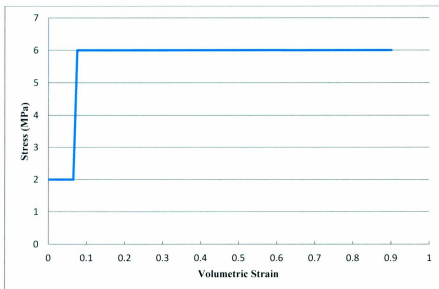


Figure 3-11: Stress – Volumetric Strain Curve in Ice Model A

The corresponding pressure-area curve is shown in Figure 3-12. It is very close to the benchmark. Note that $P_o = 5.91\text{MPa}$ in this model. It is similar to the value specified for Polar Class 1 in the URI (see Table 2-2).

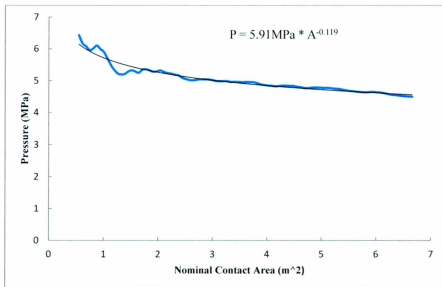


Figure 3-12: Pressure – Area Curve of Ice Model A

3.2.3 Ice Model B

Table 3-10 and Figure 3-13 show the redefined stress-strain relationship in the modified crushable foam ice model-B. Other parameters are the same as in Table 3-8. The corresponding pressure-area curve is shown in Figure 3-14. The pressure-area curves specified for Polar Class-4 and Polar Class-5 are plotted as well for a visual comparison.

Table 3-10: Stress – Volumetric Strain Relationship in Ice Model B

Volumetric Strain	0.000	0.095	1.200	0.900
Stress (MPa)	1.5	1.5	3.0	3.0

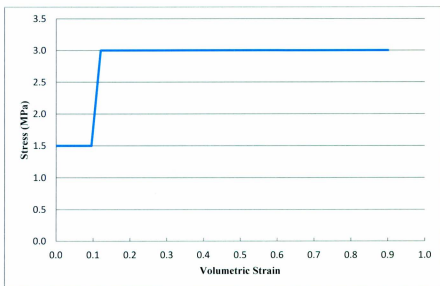


Figure 3-13: Stress – Volumetric Strain Curve in Ice Model B

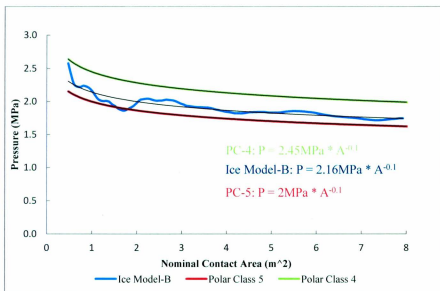


Figure 3-14: Pressure – Area Curve of Ice Model B

3.2.4 Ice Model C

The ice model C is developed by slightly altering the ice model B. Table 3-11 and Figure 3-15 show the redefined stress-strain relationship in the ice model C. Other parameters are the same as in Table 3-8. Figure 3-16 compares its pressure-area curve with the one defined for the Polar Class-3 in the URL.

Table 3-11: Stress – Volumetric Strain Relationship in Ice Model C

Volumetric Strain	0.000	0.065	0.075	0.900
Stress (MPa)	1.5	1.5	3.0	3.0

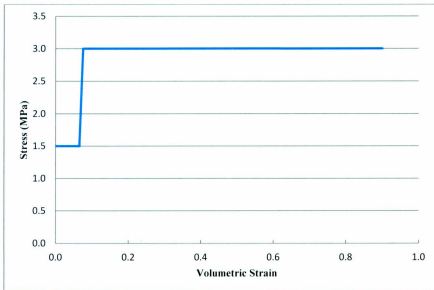


Figure 3-15: Stress – Volumetric Strain Curve of Ice Model C

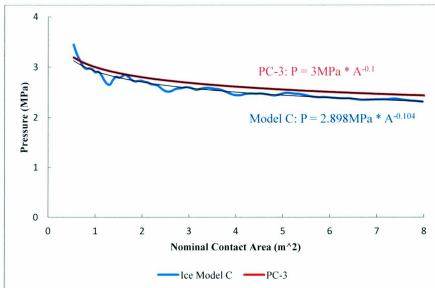


Figure 3-16: Pressure – Area Curve of Ice Model C

3.3 Ice Material Models Based on the Elastic-Plastic Material

The elastic-plastic material model available in DYNA was also evaluated. Unfortunately, no usable results were accomplished. Two of the cases that came close to the desired pressure-area curve are introduced here.

3.3.1 Ice Model D

The ice model D is a simple elastic-plastic material model. This type of material model undergoes an elastic phase then a simple linear plastic phase when under compression. Inputs for the simulation are listed in Table 3-12. Its pressure-area curve is shown in Figure 3-17.

Table 3-12: Material Properties of Ice Model D

Card ID	MAT_PLASTIC_KINEMATIC(MAT_003)			
Density	Young's Modulus	Poisson's Ratio	Yield Stress	Tangent Modulus
900kg/m^3	5GPa	0.3	5MPa	5.0

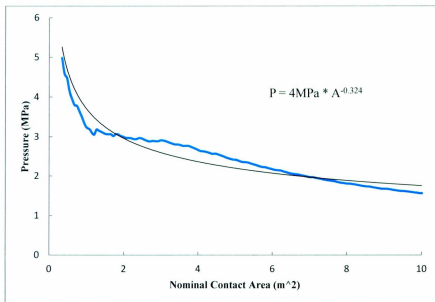


Figure 3-17: Pressure – Area Curve of Ice Model D

3.3.2 Ice Model E

Models based on the nonlinear elastic-plastic material (card MAT_24 in DYNA) were also evaluated. The ice model E is one of them. Its material properties are listed in Table 3-13. A very simple relationship of stress and plastic strain is defined (see Table 3-13). Cases with much more complicated stress-plastic strain relationships were also tested. However, their pressure-area curves are nowhere near $P = P_0 A^{-0.1}$. The ice model E is the one that has the best result. Its pressure-area curve is shown in Figure 3-18. It is clear that its pressure-area relationship cannot be accurately expressed in the form of $P = P_0 A^{-0.1}$.

Table 3-13: Material Properties of Ice Model E

Card ID	MAT_PIECEWISE_LINEAR_PLASTICITY (MAT_024)		
Density	Young's Modulus	Poisson's Ratio	Yield Stress
900kg/m ³	9GPa	0.03	0.1MPa

Table 3-14: Stress – Volumetric Strain Relationship in Ice Model E

Plastic Strain	0.000	0.1	0.11	0.96
Stress (MPa)	0.1	0.1	20	20

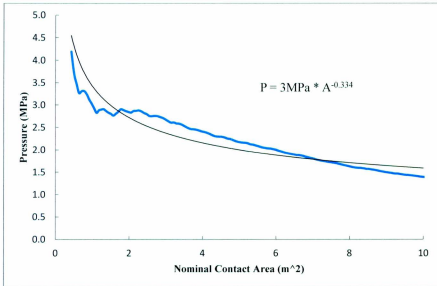


Figure 3-18: Pressure – Area Curve of Ice Model E

3.4 Summary

More than 80 different ice models have been evaluated. Their pressure-area relationships are compared with the one specified in the URI. The modified crushable foam ice model B and C are very close to the benchmark. The ice model C is chosen to be used for the rest of this study. Their relationship with the URI is shown in Table 3-15. It seems likely that ice material models corresponding to all the PC classes could be developed by modifying the material parameters of the ice model A, B and C. This needs to be further explored.

Table 3-15: Summary of Proposed Ice Material Models

Ice Material Model	Pressure-Area Relationship	Corresponding Ice Material Model Specified in the URI
A	$P = 5.91MPa \times A^{-0.119}$	Similar to PC-1: $P = 6MPa \times A^{-0.1}$
B	$P = 2.16MPa \times A^{-0.1}$	Lies in between of PC-5: $P = 2MPa \times A^{-0.1}$ and PC-4: $P = 2.45MPa \times A^{-0.1}$
C	$P = 2.898MPa \times A^{-0.104}$	Similar to PC-3: $P = 3MPa \times A^{-0.1}$
To be developed	Not available	PC-2: $P = 4.2MPa \times A^{-0.1}$ PC-6: $P = 1.4MPa \times A^{-0.1}$ PC-7: $P = 1.25MPa \times A^{-0.1}$

Ice model D and E are based on the elastic-plastic material models in DYNA. They show good agreement with general form of the desired pressure-area relationship, but are not as satisfactory as the ice model A, B and C. However, the elastic-plastic material models give users a large control over the material's stress-strain relationship, which mean they have the potential to give superior results. Moreover, the elastic-plastic material models are more robust than the crushable foam model, which allows users to simulate cases with very small contact areas, and contacts involving ice blocks with sharp edges without encountering the negative volume problems. Further development of ice models using the elastic-plastic material should be carried out.

In each case, values of the contact forces are directly given by DYNA. Values of corresponding nominal contact areas are derived in Rhinoceros®, which are larger than the actual values in DYNA. This unavoidable discrepancy is due to the nature of the contact algorithm in DYNA. As discussed in Section 1.3.4, contact in DYNA takes place before the geometries are actually in contact. This discrepancy is minimized by excluding data of small contact areas from the analysis. Taking the ice model C for example, its pressure-area curve (Figure 3-16) only contains data of contact areas larger than $0.5m^2$. If the analysis is extended to the contact area as small as $0.1m^2$, the pressure area curve will become the blue one in Figure 3-19. Its trend line is in the form of $P = 3MPa \times A^{-0.158}$ rather than $P = 3MPa \times A^{-0.104}$ as illustrated in Figure 3-16. The increase in the exponential term is to accommodate very large pressures over small contact areas. Even

so, this mathematical approximation still significantly underestimates pressures over very small contact areas. This will affect the analysis of the contact force in Chapter 5.

Another limit regarding the proposed ice models is that the analysis of each ice material model does not cover nominal contact areas larger than $10m^2$ due to the dimension of the geometric model. Simulations using bigger ice blocks should be carried out to confirm that the pressure-area relationships of the proposed ice models will still comply with the $P = P_o A^{-0.1}$ for larger nominal contact areas. Note that such large cases are unlikely for this study but may happen in real life.

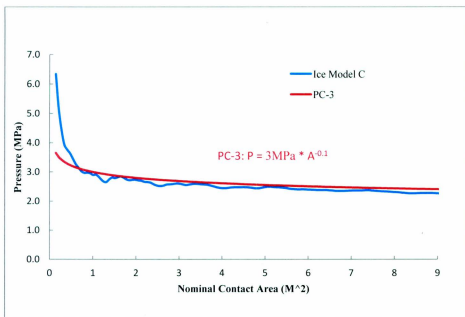


Figure 3-19: Pressure - Area Curve of Ice Model C (All Data Included)

Chapter 4 ALE Method

As discussed in the literature review, the ALE method is utilized in several studies to simulate the fluid domain in the ship-ice collision analysis. It is naturally considered as a potential approach for this thesis. However, all relevant studies included in the literature review only allowed the ship to surge and restrained it in all the other 5 DOF, while this study is more interested in modeling both the ship and ice as free floating bodies. In addition, the present study includes the ship structural response in the final solution. It will necessarily require a very refined mesh where the element size is governed by the dimensions of ship structural members. These two factors raise a concern of the computation cost of the ALE method. A set of ALE simulations similar to the model tests by Gagnon et al. (2004) are conducted to explore this concern. This revealed that the ALE is not a practical approach for this study. The ALE method was however used to estimate the added mass and damping coefficients. These were then used to help develop user-defined-curve-functions to replace the ALE method.

4.1 Simulations for Evaluating the Computation Cost

4.1.1 Geometric Model

The experiments by Gagnon et al. (2004) used a 1:41 scale tanker model that was 7.20 m in length, with a beam of 1.16m, a depth of 0.44m, and a draft of 0.37m. Cylindrical, pyramid, and spherical ice masses of various dimensions were used as ice models. In a typical test, the ship began to move forward (the +x-direction) while the ice floe was held at its neutral buoyancy position. There was a separation between the ice and ship in the

transverse direction (y-direction) so that no collision would occur. The separation is measured as the distance between the CG of the ship to the CG of the ice mass in the transverse direction. After the ship accelerated from zero to the designed speed, the ice was fully released. The surge and sway motions of the ice were measured as the ship passed by at a constant speed. The sway motion of the ice was well recorded but data of surge motion were not available for all runs. Gagnon et al. (2006) conducted an ALE simulation of one test that involved a spherical ice mass. It showed a good agreement with the experiment in the sway motion.

To evaluate the computation cost of the ALE method, several simulations similar to the experiments described above have been conducted. Each simulation is in full scale rather than model scale. Figure 4-1 is the plane view showing the dimensions of the full scale simulation where all units are in meters. The geometric model of the ship (red) was provided by Dr. Jungyong Wang (Wang, 2011). It is the same one used in the experiments by Gagnon et al. (2004) and the numerical simulation by Gagnon et al. (2006). The radius of ice (blue) is 24.6m and the separation between ship and ice is 59m. They are directly scaled from the experiment. The distance from the tip of the bow to the center of the spherical ice in the x-direction is about 27m. In the vertical (z-) direction, the ship is placed at its designed draft. The ice is located at the position of neutral buoyancy. The water domain (cyan) is 410m in length, 164m in width, and 69.7m in depth. The air domain has the same length and width as the water domain but only 12.3m in height. The whole ALE domain (water and air) is a $410m \times 164m \times 82m$ box. Note that the number of

elements is dominated by the size of the ALE domain so it is built as small as possible but with enough space for the floating bodies to move around. The 3D model in DYNA is shown in Figure 4-2 where the air domain is hidden and the exterior yellow layer is the ambient water domain for a reservoir boundary condition that will be explained later. The element size in Figure 4-2 is 4.1m.

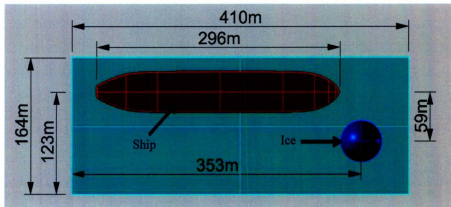


Figure 4-1: Top View of the Geometric Model in Rhinoceros®

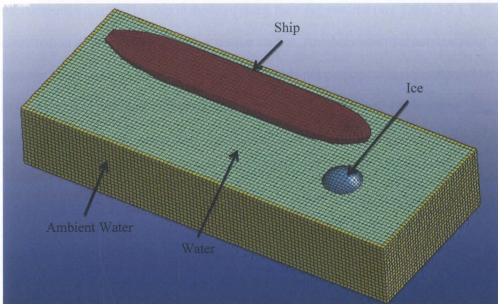


Figure 4-2: 3D Model in DYNA

4.1.2 Material Models

In ALE simulations, material models for water and air (including ambient entities) are standard and straightforward as the water domain develops a proper hydrostatic distribution. Users should strictly follow the DYNA's instructions (LSTC, 2010).

Detailed information is presented here. The elastic-plastic material is chosen for modeling ice (see Table 3-12). The ice model C from Chapter 3 is not used because simulations presented here were conducted before the investigation of the ice models introduced in Chapter 3. The elastic-plastic ice and the crushable foam ice share the same Young's modulus and material density, the dominant factors in the fluid structure coupling in the ALE method. Therefore the difference in ice material should not affect the evaluation of

the computation cost. The ship is modeled using the rigid material (see Table 3-2). This combination is very common in other similar studies. Another reason for not modeling both the ship and ice as rigid is that rigid elements do not participate in the computation of time step (see Section 1.3.2). If the purpose of the simulation is to validate the experiments mentioned earlier, both the ship and ice should be treated as rigid to save computation time.

4.1.3 Element Choices

In all simulations in this chapter, the ship is modeled using shell elements and ice is analyzed using the default solid elements (see Table 3-4). Choices for elements of water and air follow the standard instruction of the ALE method. They are summarized in Table 4-1. The proper element size is determined via a mesh convergence study. It will be discussed in Section 4.2.6.

Table 4-1: Element Choices for the ALE Simulations

Part	Element	Formulation Option	Ambient Type
Water	Solid	11	0
Air	Solid	11	0
Ambient Water	Solid	11	4
Ambient Air	Solid	11	4

4.1.4 Boundary and Initial Conditions

The simulation time is 15 seconds for each analysis. During the first second, both the ship and ice are held at their initial positions when the water domain develops a proper hydrostatic distribution. At 1 second, the ice is fully released in all 6 DOF. At the same time, the ship starts moving forward at the prescribed speed but is still restrained in the other 5 DOF. This is similar to the model test. The ship accelerates from 0 m/s to 5m/s from 1 second to 2 seconds. Starting from 3 seconds, the ship moves forward at a constant speed of 5m/s until the end of the simulation. The ship's forward speed is not scaled from the experiment because the purpose of the simulation is to evaluate the computation cost rather than validating the experimental results.

There are two types of boundary conditions available for modeling water using DYNA. They are referred to as the "swimming pool" boundary condition and the reservoir boundary condition. A "swimming pool" boundary condition allows the waves generated by floating bodies to bounce back and forth between the wall-like boundaries. This phenomenon significantly disturbs the hydrostatic distribution in the fluid domain and thus contaminates the results. Unless a finite sized "swimming pool" is desired, a reservoir boundary condition should be applied by adding ambient layers to the regular fluid domain. The hydrostatic distribution in the ambient layers must be defined using the *ALE_AMBIENT_HYDROSTATIC card. Waves generated by floating bodies will flow into the ambient layers and not bounce back. In other words, the extra ambient layers transfer a finite fluid domain to a pseudo infinite one without using more elements or

increasing the size of the fluid domain. Figure 4-3 shows the ALE domain with ambient layers. Part of the domain is cut away for a clear demonstration. The water domain (blue) is surrounded by the ambient water layer (yellow) on all four sides and the bottom. The air domain (red) is surrounded by the air ambient layer (green). There is no ambient layer on top of the air domain simply because it is not necessary. The reservoir boundary condition is used in all simulations presented in this chapter.

Initial conditions for the ALE domain are defined strictly following DYNA's instructions for a realistic hydrostatic pressure distribution that takes about 0.5s to develop. Note that ambient entities and regular ALE elements require separate inputs.

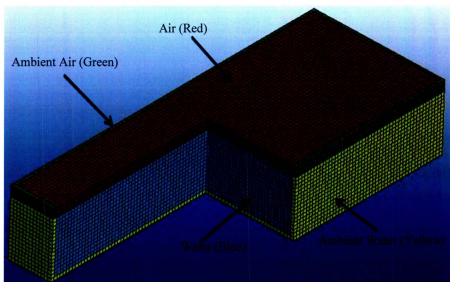


Figure 4-3: the ALE Domain including Ambient Layers

4.1.5 Other Inputs

Gravity is included in the analysis. Hydrostatic and hydrodynamic forces are included using the ALE method. When defining the fluid-structure coupling force, the PFAC value is carefully calibrated so that each floating body is in neutral buoyancy at the initial position. In each simulation, damping is applied to the water and air domains for the first 0.5 seconds. It helps the ALE domain to form the realistic hydrostatic pressure distribution faster. There is no ship-ice contact in each simulation.

4.1.6 Mesh Convergence

The convergence study is conducted by observing the surge, sway, and heave motion of the ice in simulations using various element sizes. Results are shown in Figure 4-4, Figure 4-5, and Figure 4-6. It is obvious that the convergence in the sway motion is excellent. Convergence in the surge motion is acceptable when the element size is smaller than 4.1m. Convergence is not reached for the heave motion. Note that the simulation reported by Gagnon et al. (2006) contained about 2 million elements and had good agreement with the model test in the sway motion. So overall, the mesh convergence is acceptable. The number of elements and the total computation time for each case are summarized in Table 4-2. It is reasonable to conclude that 1.33m is an appropriate element size. Further refining the mesh may give better convergence in all three motions, but it will also significantly add to the total computation cost, which is the biggest concern regarding the use of the ALE method.

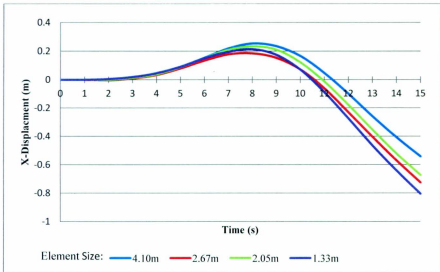


Figure 4-4: Convergence of the Ice Surge Motion

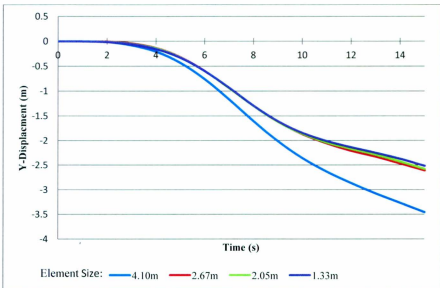


Figure 4-5: Convergence of Sway Motion of Ice

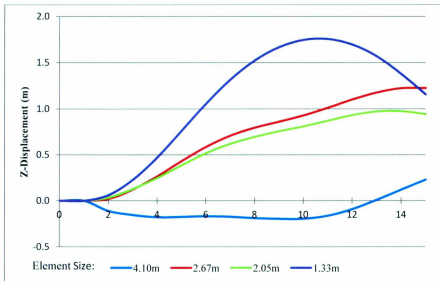


Figure 4-6: Convergence of the Ice Heave Motion

Table 4-2: Summary of the Mesh Convergence Study

Case No.	A	B	C	D
Mesh Size	4.10m	2.67m	2.05m	1.33m
No. of Elements	94,280	313,696	726,354	2,401,832
Computation Time	1hr 16min	4hr 17min	12hr 34min	50hr 23min
No. of Compute Nodes	4	4	4	4

Note: All simulations are solved on STePS2 Cluster (see Appendix A) which has 8 cores in each compute node.

4.1.7 Evaluation of the Computation Cost

The total computation cost for an ALE simulation depends on four factors: element size, the total number of elements, the contact model, and boundary conditions. In each case presented in this chapter, the ALE domain is built as small as possible but with enough space for the ship and ice to move around. One floating part (ice) is assigned with 6 DOF while the other one (ship) is only free to move in the surge direction. Contact is not included. Case D, where the element size is 1.33m, contained about 2 million elements and took about 50 hours to solve.

Assuming a very small ship-ice model that is one third in size of the model presented above is used, the dimension of the ALE domain will become $100m \times 50m \times 20m$. With the same element size as Case D, the total element number will be about 43,000. This number is about 1.8% of Case D. If a 5-second simulation time (1/3 of Case D) is needed for a ship-ice collision analysis, then the total computation time can be roughly estimated as $50hr \times 1.8\% \times \frac{1}{3} = 18 \text{ min} = 0.3 \text{ hr}$. However, this is for the simulation using solid elements of 1.33m in length. In a ship-ice collision analysis involving local structural response, the element sizes of the ship, ice, and the ALE domain should be similar to each other for accurately modeling contact and coupling forces. The element size will necessarily be dominated by the smallest parts, which are the structural members of the ship. The proper element size should be in the neighborhood of 0.15m. For the same ALE simulation whose dimension is $100m \times 50m \times 20m$, the total number of elements will be about $100 \times 50 \times 20 \div 0.15^3 \approx 29.6 \text{ millions}$. Recalling equations [3.1] and [3.4]

which show that computation time step is proportional to element length, the total estimated computation is $0.3hr \times \frac{29.6 \text{ millions}}{43,000} \times \frac{1.33m}{0.15m} \approx 1831 \text{ hours} \approx 76 \text{ Days}$.

Including the contact model and more DOF in the analysis will increase the computation time even more. Although using a non-uniform mesh may cut the number of elements in half, the total computation cost will still be about 38 days. This is not an efficient or practical engineering solution.

A more cost efficient approach, the user-defined-curve-function, can be used to model the hydrodynamic effects and hydrostatic forces. The ALE domain can be completely eliminated and this reduces the number of elements by about 80%. It also makes the numerical model much simpler. Using user-defined-curve-functions to account for hydrodynamic forces requires added mass and damping coefficients as inputs. These values can be derived from model tests, analytical solutions, numerical simulations, or empirical estimations. In the present study, ALE simulations are used to calculate them. The detailed discussion of implementing user defined function is addressed in Chapter 5.

4.2 Oscillatory Analysis vs. Transient Analysis

There are two methods for estimating added mass terms: the oscillatory analysis and the transient analysis. Taking the heave added mass for example, the oscillatory method assigns an initial heave displacement to the floating body and then lets it oscillate in the water. The heave added mass coefficient a_{33} can be solved using Equation 4-1:

$$a_{33} = \frac{T^2 k}{4\pi^2 m} - 1 \quad \text{Equation 4-1}$$

where T is the oscillatory period, m is the mass of the floating body, and k is the heave stiffness.

The transient analysis solves the same problem by applying a force in the heave direction to the floating body. The heave added mass coefficient a_{33} is given as:

$$a_{33} = \frac{F}{a} \frac{1}{m} - 1 \quad \text{Equation 4-2}$$

where F is the external force applied, a is the acceleration due to the force, and m is the mass of the floating body. This section will compare the two approaches using ALE simulations.

4.2.1 Geometric Model

Simulations using the transient and oscillatory methods have the same geometric model. It is shown in Figure 4-7 where the air domain is hidden. The blue part is the water domain and the yellow part is the ambient water layer. Dimensions of the ALE domain are in Table 4-3. The diameter of the semi-submerged sphere (red) is 6m. The element size in the figure is 0.5m.

Table with 4 columns: Length (m), Width (m), Height (m), and Volume (m³)

	Length (m)	Width (m)	Height (m)
Water Cube (m)	10	10	10
Ice Cube (m)	10	10	9

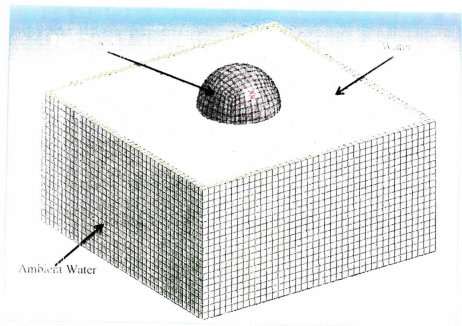


Figure 10.10: Ice in Water

4.2.2 Material Models

The sphere is modeled as a rigid body using shell elements. Its density is set at 2960.10 kg / m^3 so that it is in a state of neutral buoyancy when it is semi-submerged.

4.2.3 Element Choices

Element choices for the ALE Domain are the same as in Table 4-1. The semi-submerged sphere is meshed using shell elements rather than solid elements to reduce the total number of elements. Information of the shell elements is available in Table 3-4. The thickness of each shell is 0.1694m. The element size is much smaller than that in Section 4.1, therefore no mesh convergence study is conducted for this analysis.

4.2.4 Boundary and Initial Conditions

The reservoir boundary conditions are applied to the ALE domain in all simulations. The hydrostatic pressure distribution properly develops in about 0.5 seconds.

All 6 DOF on the sphere are constrained for the first second. Starting from 1 second, there are two options for the boundary condition on the sphere. The first option is to set the sphere to be completely free floating. A few simulations suggested that this type of boundary condition makes it very difficult to analyze the heave motion for two reasons. First, since the perfect PFAC value is impossible to find, the sphere will always oscillate around its neutral buoyancy position. Besides, motions in other DOF tend to couple with the heave. This influence is especially significant when the heave is not the dominant

motion, i.e., a small initial heave displacement or a small external force is applied to the sphere. Some of the simulations report unrealistically negative values for the heave added mass. Therefore the other type of boundary condition is chosen. The sphere is restrained in all DOF except the one that is being investigated; therefore, the added mass in each DOF is evaluated independently. Note that when the applied external force is relatively large, these two boundary conditions show similar results.

In the oscillatory analysis of the heave added mass, the sphere is assigned a prescribed heave motion for the first 3 seconds (see Figure 4-8). At 3 seconds, it is released to be free in the heave motion but fixed in all the other DOF. In simulations using the transient analysis, there is no prescribed motion for the sphere. The sphere is fixed in all 6 DOF during the first second, and then it is released in the heave motion but still restrained in all other 5 DOF.

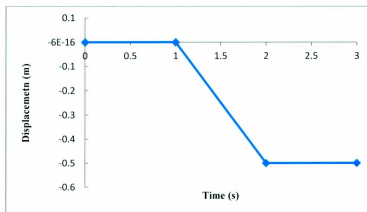


Figure 4-8: Prescribed Heave Motion of the Sphere in the Oscillatory Analysis

4.2.5 Loading Conditions

Gravity is included in all simulations. There is no other load in the simulation using the oscillatory method. Multiple simulations using the transient approach are carried out. In each simulation, a force is applied to the sphere in the $-z$ -direction (downwards) to push it into the water. The force ramps up from zero to the designed value in 0.009 seconds (from 2.001 to 2.01 seconds). The value of the force varies over simulations to investigate if the magnitude of the force affects the heave added mass.

4.2.6 Added Mass using the Oscillatory Analysis

The time history of the heave motion of the sphere is shown in Figure 4-9. The oscillatory period is about 3.65 seconds. The mass of the sphere is $56,438.8 \text{ kg}$. Its heave stiffness is $276,394 \text{ N/m}$. Substituting those values into Equation 4-1, the heave added mass coefficient is solved as 0.654. The time history suggests that damping is very small. A calculation using the logarithmic decrement method suggests that the damping ratio is approximately 3%.

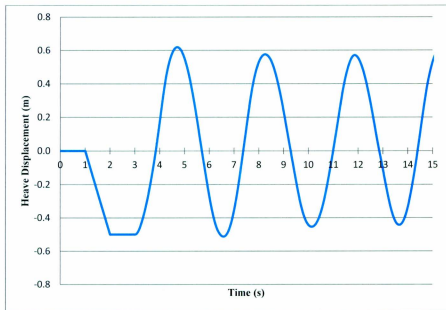


Figure 4-9: Heave Motion of the Semi-Submerged Sphere

4.2.7 Added Mass using the Transient Analysis

Results of the simulation where the external force is about 22 times larger than the sphere's weight are shown in Figure 4-10. After the force is applied, the sphere acquired a large acceleration in the $-z$ -direction. Buoyancy increases as the sphere is pushed into deeper water, which causes the acceleration to decrease. At about 2.1 seconds, part of the sphere is pushed out of the fluid domain so the buoyancy begins to decrease. The decrease of the acceleration is consequently slowed down. Eventually, the sphere is completely pushed out of the water. This results in zero buoyancy and hence a constant acceleration due to gravity and the force applied. In the solution, both the force and the

acceleration are negative values. The minimum value of the acceleration is given by DYNA's outputs. The heave added mass coefficient is solved using Equation 4-2. Note that before the force is applied, the sphere already has a small heave acceleration due to the unstable hydrostatic force. This noise is due to the nature of the ALE simulation and is taken into consideration during the analysis. All results from all simulations are summarized in Table 4-4 and Figure 4-11. It is obvious that the heave added mass in this analysis is independent of the force applied.

Table 4-4: Influence of the Magnitude of the Force on the Heave Added Mass

Magnitude of the Force (KN)	30	54	120	567	1,206	6,030	12,060	18,090
Force/Body-weight Ratio (%)	5	10	22	103	218	1090	2181	3271
Heave Added Mass Coc. (%)	8.9	6.1	8.7	10.2	8.7	9.1	9.0	9.4

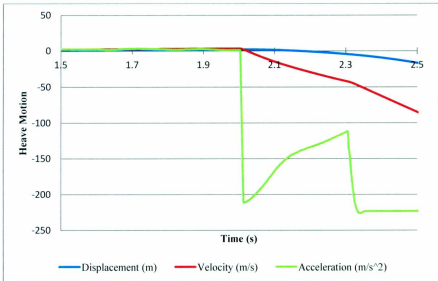


Figure 4-10: Time History of the Semi-Submerged Sphere's Heave motion

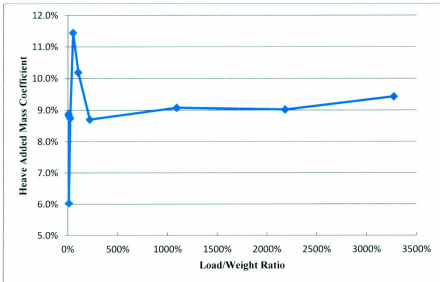


Figure 4-11: Influence of the Magnitude of the Force on the Heave Added Mass

4.2.8 Comparison

It is clear that the added mass estimated by the oscillatory method is larger than that given by the transient approach. In other words, “water” in DYNA is more responsive and sensitive to the low-frequency motion of the floating body. A similar phenomenon is also reported in many time-domain studies on the oscillating hemisphere. They are summarized in Table 4-5 where cases of very-low frequencies share a similar nature with the oscillatory analysis, and cases featuring very-high frequencies correspond to the transient analysis.

Table 4-5: Heave Added Mass Coefficients at Very-Low Frequencies and Very-High Frequencies on the Unit Hemisphere

Very-Low Frequencies	Very-High Frequencies	Reference
0.8	0.4	Sierevogel (1998), Prins (1995)
0.8	0.5	Korsmeyer et al. (1989), Liapis (1986)
0.83	0.5	Hulme (1982)
0.83	0.5	Storti et al. (2004)

It is apparent that the heave added mass estimated using the ALE method is significantly smaller than those given by the time-domain studies. This discrepancy is most likely due to the nature of the fluid-structure coupling in DYNA. As discussed in Section 1.3.3, it computes the coupling force using a penalty method, i.e., the force is always a function of the displacement. While in reality, the added mass is in phase with acceleration or deceleration. Results using the time-domain analysis are more trustworthy.

For the ship-ice collision analysis, the contact force is more like an impulse force, i.e., a very-high frequency load. Thus, the transient approach is more suitable for estimating the added mass terms.

4.3 Estimation of Added Mass and Damping Coefficient

ALE simulations following the transient approach are conducted to estimate the added mass and damping coefficients of the ship and ice. They will be input into user-defined-curve-functions in the next chapter to replace the ALE method.

4.3.1 Geometric Model

The ship and ice are analyzed in separate simulations. Geometric models of the ship and ice are the same as in Section 3.1.1 except that ice edges are not rounded. The dimension of the water domain is $80m \times 24m \times 8m$. The dimension of the air domain is $80m \times 24m \times 4m$. The 3D models are shown in Figure 4-12 and Figure 4-13 where the air domain is hidden.

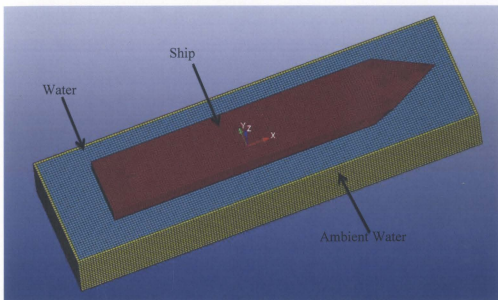


Figure 4-12: 3D Model for Estimating the Added Mass Coefficients on the Ship

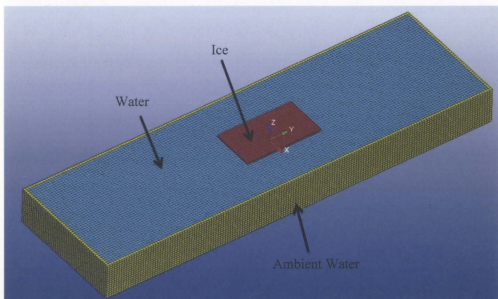


Figure 4-13: 3D Model for Estimating the Added Mass Coefficient on the Ice

4.3.2 Material Models

Both the ship and ice are modeled using the rigid material since the deformation is irrelevant. Material properties of the ship are the same as in Table 3-2. Since the ice block is meshed using shell elements, its material density is set at $6121.69 \text{ kg} / \text{m}^3$ so that it has the same mass and same neutral buoyancy position as if it was a solid block. The change in the moment of inertia due to this adjustment is taken into consideration in all the calculations performed in this chapter.

4.3.3 Element Choices

Element choices of the ALE domain are the same as in Table 4-1. Both the ship and ice are modeled using the same shell elements as those in Table 3-4.

4.3.4 Boundary and Initial Conditions

Boundary conditions on the ALE domain are the same as the ALE simulations presented earlier. Boundary conditions on the ship and ice are summarized in Table 4-6.

Table 4-6: Boundary Conditions on the Ship and Ice

Case	From 0 second to 1 second	From 1 second and onwards
Surge	All 6 DOF Restrained	Free in Surge, Restrained in all other DOF
Sway	All 6 DOF Restrained	Free in Sway, Restrained in all other DOF
Heave	All 6 DOF Restrained	Free in Heave, Restrained in all other DOF
Roll	All 6 DOF Restrained	Free in Roll, Restrained in all other DOF
Pitch	All 6 DOF Restrained	Free in Pitch, Restrained in all other DOF
Yaw	All 6 DOF Restrained	Free in Yaw, Restrained in all other DOF

4.3.5 Loading Conditions

In each simulation, a force or moment is applied to the floating body (ship or ice) for 2 seconds (from 6 seconds to 8 seconds). When investigating the translational motion (surge, sway and heave), the magnitude of the force is about 10% of the body weight to generate an acceleration of $1m/s^2$ if there is no “water”. When studying the rotational motion (roll, pitch and pitch), the moment applied to the body will generate a rotational acceleration of $0.1 rad/s^2$ if there is no “water” in the analysis. Values of the applied loads are summarized in Table 4-7. Note that when analyzing the ship’s heave motion, the force is applied to push the ship downwards into the water, but when investigating the ice’s heave motion, the force is applied in the positive z-direction to lift the ice up. This is because a large force downwards makes the ice completely submerged and hence difficult to observe the heave motion.

Table 4-7: Values of Applied Loads

Floating Body	Heave	Roll	Pitch
	Value (KN)	Value (MNm)	Value (MNm)
Ship	-3,037	8,653,020	101,849,000
Ice	453	1,290,580	564,483

4.3.6 Ship's Added Mass and Damping Terms

The time history of the ship heave motion is shown in Figure 4-14. The ship is released at 1 second. The heave acceleration begins to vary dramatically for the next 2 seconds due to the nature of the PFAC value. It then becomes more stable but still oscillates a bit. At 6 seconds, a force is applied to the ship and generates a large acceleration in the $-z$ -direction. It pushes the ship downwards into the water. The increasing buoyancy causes the heave acceleration to decrease. The force is removed at 8 seconds and buoyancy immediately dominates. It gives the ship a large positive acceleration. After that, the ship starts oscillating in the water. The magnitude of the acceleration at 6 seconds is 0.8179 m/s^2 . Using Equation 4-2 computes the heave added mass coefficient as 0.198. The damping ratio is calculated using the logarithmic decrement method. Its value is 0.722. Results are summarized in Table 4-8.

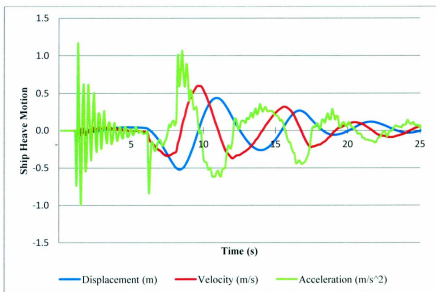


Figure 4-14: Time History of the Ship Heave Motion

The time history of the roll motion is shown in Figure 4-15. A moment about the x-axis is applied to the ship at 6 seconds to initiate the roll motion. After it is removed at 8 seconds, the restoring force causes the ship to oscillate. The acceleration due to the applied moment is 0.0898 rad/s^2 . The roll added mass coefficient is calculated as 0.114 using Equation 4-2. The oscillation in Figure 4-15 contains two crests and two troughs. The first crest and trough have relatively large amplitudes. The second crest and trough are much smaller. Damping barely exists if only the first crest and trough are analyzed. However, the whole oscillation suggests that the system is heavily damped compared to real-life roll motion. The damping ratio is calculated as 0.78 using the logarithm decrement method. Results are summarized in Table 4-8.

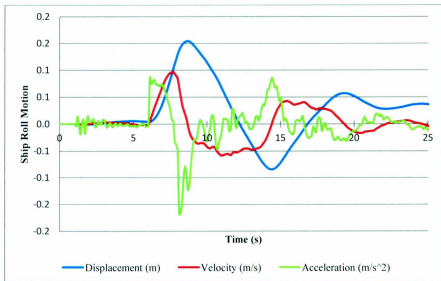


Figure 4-15: Time History of the Ship Roll Motion

Pitch motion is investigated in the same way as the roll motion. Its time history is shown in Figure 4-16. A moment about the y-axis is applied to the ship at 6 seconds to trigger the pitch motion. After it is removed at 8 seconds, the ship begins to oscillate about the y-axis. The acceleration due to the applied moment is 0.0871 rad/s^2 . Applying Equation 4-2 gives the pitch added mass coefficient as 0.148. The logarithm decrement suggests the damping ratio is 0.442. Results are summarized in Table 4-8 as well.

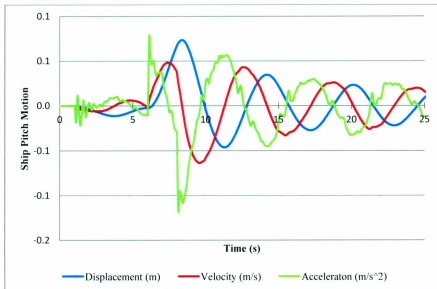


Figure 4-16: Time History of the Ship Pitch Motion

Added mass coefficients in the surge, sway, and yaw motions are estimated in the same manner except that damping did not exist in those three motions since there is no oscillation. Results are summarized in Table 4-8.

Table 4-8: Added Mass and Damping Terms of the Ship

Term	Surge	Sway	Heave	Roll	Pitch	Yaw
Added Mass Coe.	0.178	0.140	0.198	0.114	0.148	0.113
Damping Ratio	N/A	N/A	0.722	0.787	0.442	N/A

4.3.7 Ice Added Mass and Damping Terms

Added mass and damping terms of the ice are analyzed in the same way. Time histories of the heave, roll, and the pitch motion are shown in Figure 4-17, Figure 4-18, and Figure 4-19 respectively. Each of them demonstrates a similar pattern to the corresponding time history of the ship motion. Note that the oscillation in the heave motion is very unstable. Values of the first two troughs are then used to calculate the damping ratio. Added mass coefficients in the surge, sway, and yaw motions are estimated as well. All the results are summarized in Table 4-9.

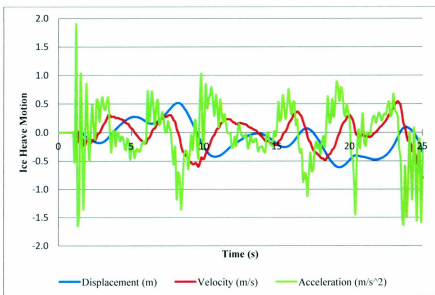


Figure 4-17: Time History of the Ice Heave Motion

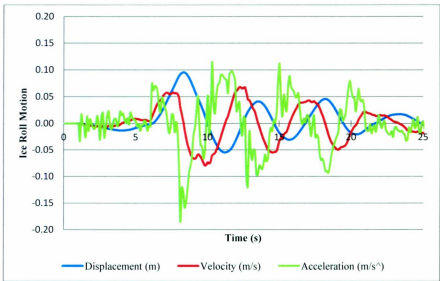


Figure 4-18: Time History of the Ice Roll Motion

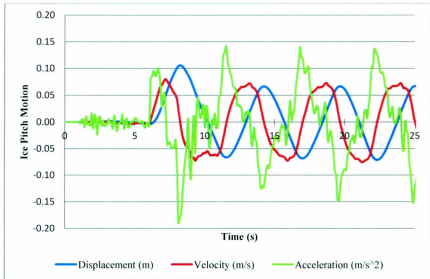


Figure 4-19: Time History of the Ice Pitch Motion

Table 4-9: Added Mass and Damping Terms of the Ice

Term	Surge	Sway	Heave	Roll	Pitch	Yaw
Added Mass Coe.	0.226	0.165	0.193	0.247	0.147	0.149
Damping Ratio	N/A	N/A	0.511	0.354	0.072	N/A

4.3.8 Comparison

Table 4-10 compares the added mass terms estimated in the previous sections with the ones given by the software Direct Design for Polar ships (DDePS), a solution that is based on the Popov's derivation (Popov et al. 1967) and further developed by Daley et al. (2007, 2008, 2009a). Applications of DDePS can also be found in Daley et al. (2009b, 2010), and Kendrick et al. (2009). Note that DDePS and Popov's estimations are based on experimental and empirical values rather than the transient analysis. Therefore, the discrepancy in the results is expected. The added mass coefficients of the ship given by DDePS are very reasonable and agree well with the common knowledge of the added mass of ships. They are also in the same order of magnitude with the values suggested by DYNA. In terms of the ice block, estimations given by these two solutions are also in the same order of magnitude except for the heave and pitch added mass coefficients. It is difficult to conclude which solution gives the more accurate answer since there are no other studies to compare with for this particular case.

Table 4-10: Added Mass Coefficients Calculated by DDePS (1967) and Present Work

Added Mass Coefficients	Ship		Ice	
	DDePS	Present Work Using DYNA	DDePS	Present Work Using DYNA
Surge	0.000	0.178	0.827	0.226
Sway	0.800	0.140	0.464	0.165
Heave	0.675	0.198	1.443	0.193
Roll	0.250	0.114	0.250	0.247
Pitch	0.741	0.148	2.164	0.147
Yaw	0.575	0.113	0.328	0.149

4.4 Summary

The ALE method has been shown to be impractical in simulating the fluid domain in the ship-ice collision analysis. It is replaced with user-defined-curve-functions in Chapter 5, which is an approach that requires the added mass and damping coefficients as inputs. Those coefficients are evaluated using the transient analysis in ALE simulations.

As shown by studies using the time-domain analysis, the transient analysis and oscillatory analysis give very different estimations for added mass coefficients. This is confirmed by simulations in DYNA. However, there is a discrepancy in the results due to the nature of the ALE method. As mentioned earlier, DYNA uses the penalty based algorithm to determine the fluid-structure coupling force, i.e., the force is a function of the penetration

depth between the body and water. Since the added mass and damping are in phase with the acceleration and velocity respectively, DYNA is not the ideal tool to estimate them.

The added mass coefficients given by DDePS are very different from those estimated by DYNA. This is expected since the DDePS solution is based on empirical values, while the DYNA's results are derived from transient analyses. Although the ship-ice contact is a transient process, the added mass coefficient given by DYNA is not accurate due to the nature of the program. It is difficult to determine whether the answer given by DYNA or DDePS is closer to the true value since there are no other studies to compare with for this particular case. However, in Chapter 5, added mass coefficients and damping ratios derived in this section using DYNA are used to calculate inputs for modeling water using defined-curve-functions. There are two reasons for choosing values given by DYNA. Firstly, the practice performed here is replacing the ALE method with curve functions. Therefore, inputting values given by the ALE method to the curve function can give the results similar to simulations using the ALE method. Another reason is that DDePS is a very quick solution that only takes a few minutes to finish one analysis. It is much simpler to input various sets of added mass coefficients into DDePS and compare the results with the DYNA solution than the other way round. If added mass coefficients suggested by more reliable sources are available, such as experiments, and CFD simulations, they should be adopted into the user-defined-curve-functions.

Another factor that may contaminate the result is the PFAC value. It must be carefully calibrated for each simulation. If the geometry model, the element size, or any other input related to fluid-structure coupling is modified, the PFAC value must be recalibrated. This is a very time consuming process that may take hours or even days depending on the mesh and complexity of the simulation.

Chapter 5 Ship Ice Collision Force

This chapter discusses modeling the global ship-ice contact force. Restoring forces are included in the solution by modeling the water domain as a spring system with user-defined-curve-functions. Several ship-ice glancing cases are analyzed. Results are compared with calculations using DDePS.

5.1 Defined-Curve-Functions

This section discusses how to implement the *DEFINE_CURVE_FUNCTION card to model the water instead of simulating the water domain using solids elements. Modeling the restoring forces is covered in Section 5.1.1. Modeling the drag force and the added mass effect is discussed in Section 5.1.2.

5.1.1 Restoring Forces

As mentioned in Chapter 1, the *DEFINE_CURVE_FUNCTION card defines a curve where the abscissa is and can only be time and the ordinate is expressed by a function of other curve definition, forces, kinematical quantities, intrinsic functions, interpolating polynomials, or combinations thereof. The ordinate in a user-defined-curve-function is updated at each time step as the simulation proceeds. Therefore the ordinate is a function of time. Users can then define a force (or forces) as a function of the ordinate value. For example, a force can be defined as a function of the displacement. This displacement is given as the ordinate in a user-defined-curve-function, and is updated over time by

DYNA. Three of available curve functions are used in this study to account for restoring forces (LSTC 2007a):

- DZ (node N): It reports the z-translational displacement of node N in the global coordinate system.
- AX (node N): It reports the rotational displacement of the node N about the x-axis in the global coordinate system. A local coordinate system must be defined at the node N.
- AY (node N): It reports the rotational displacement of the node N about the y-axis in the global coordinate system. A local coordinate system must be defined at the node N.

Assuming the node N is the center of gravity (CG) of a floating body and its local coordinate system shares the same orientation with the global coordinate system, the three functions (DZ, AX and AY) will update the values of heave, roll, and pitch at each time step. In a finite element analysis, calculation time step is generally very small. This implies none of those values will vary significantly at each time step. Therefore, they can be used to calculate restoring forces using the hydrostatic theory if small motions are assumed. The stiffness in heave, roll, and pitch are also required to define restoring forces in DYNA. They can be easily calculated with the outputs from Rhinoceros®. In summary, this approach calculates restoring forces using the hydrostatic theory at each time step. However, those forces are time dependent and applied dynamically to the floating body in the global context. The added mass coefficients estimated in Section 4.3 are adopted to

calculate the damping coefficients. The three curve-functions have been tested and proved to be responsive to the motion of the body.

5.1.2 Implementation

Implementation of user-defined-curve-functions will be explained using the ice block from Section 3.1 as an example. The boundary condition (see Figure 3-6) on it is removed so it becomes a free-floating body.

Step 1: Creating a rigid part on the non-rigid body. The rigid part is for reference purpose so that a local coordinate system can be built on the ice. The rigid part could be very big or very small as long as it does not affect the overall behavior of the non-rigid body. It may contain as few as one element. In this case, elements that are far away from the potential contact region are redefined as rigid using the “move” command in DYNA. The first step is shown in Figure 5-1 where the ship is in red, the crushable ice is in blue, and the redefined rigid ice is in green. This step is not necessary if the whole body is modeled as rigid in the first place.

Step 2: Creating the local coordinate system. It is shown in Figure 5-2. The CG of the ice block can be determined using the “measure inertia” command in DYNA. Its global coordinates are used to create a node (Node 138003 in Figure 5-2) as the origin of the local coordinate system. Node 138004 and node 138005 are created to define the x- and y-axes of the local coordinate system. The z-axis is automatically determined following

the right-hand rule. The local coordinate system is defined to share the same orientation with the global one to make it convenient to define loads later. Note that all three newly created nodes are massless so they will not affect the physics of the model. The local coordinate system is integrated into the ice block using the *CONSTRAINED_EXTRA_NODES_NODE card which ties the three nodes to the rigid part of ice. Note that this card only works for rigid bodies and this is why a rigid part must be created first.

Step 3: Defining restoring forces with user-defined-curve-functions. Load definitions of restoring forces are listed in Table 5-1. As mentioned earlier, functions DZ(138003), AX(138003), and AY(138003) are user-defined-curve-functions reporting heave, roll, and pitch displacements of the node 138003 (CG of the ice). They are multiplied with the stiffness, which are computed using outputs from Rhinoceros®, to define the restoring forces. Each restoring force can be applied either as a point load to the CG or distributed evenly among all the nodes on the ice. These two approaches lead to very similar results. In this thesis, each restoring force is applied as a point load for simplicity.

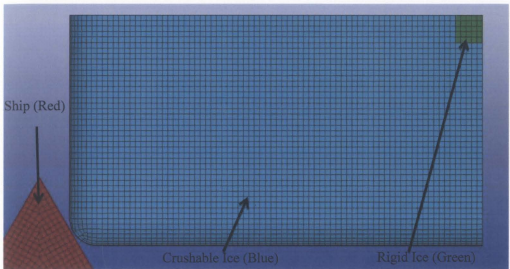


Figure 5-1: Creating a Rigid Part

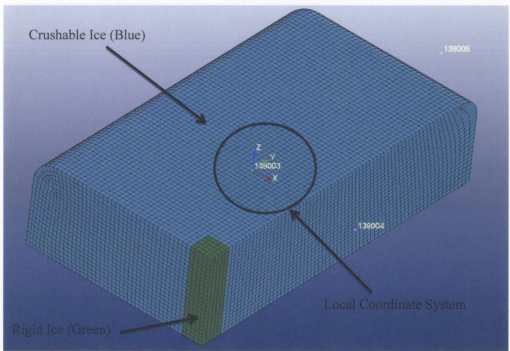


Figure 5-2: Creating the Local Coordinate System

Table 5-1: Load Definition for Restoring Forces

Motion	Stiffness	Load Definitions for Restoring Forces
Heave	4,538,321	-4,538,321*DZ(138003)
Roll	23,631,412	-23,631,412* AX(138003)
Pitch	6,661,882	-6,661,882*AY(138003)

Note: Node 138003 is the CG of the ice.

Step 4: Defining damping. Damping for each individual body is defined using the DAMPING_PART_MASS_SET card in DYNA. Its algorithm does not include mass in the calculation of damping coefficients. For instance, the theory of dynamics estimates the critical damping coefficient as:

$$b_c = 2\sqrt{km} \quad \text{Equation 5-1}$$

where k is the stiffness and m is the mass. DYNA uses a concept of critical damping factor, which is calculated as:

$$D_s = 2\omega = 2\sqrt{\frac{k}{m}} = \frac{b_c}{m} \quad \text{Equation 5-2}$$

where ω is oscillatory frequency. Note that m is the sum of actual mass and the added mass in this thesis. The damping factor D for DYNA input is calculated as:

$$D = \zeta D_s \quad \text{Equation 5-3}$$

where ζ is the damping ratio derived in Section 4.3. In this thesis, the added mass coefficients estimated by DYNA are used to calculate the total mass and damping coefficients. Their values are listed in Table 4-10.

5.1.3 Drag and Added Mass

Drag forces can be applied to the body using curve functions associated with velocities terms such as VX, VY, VZ, WX, WY, and WZ. They can be implemented in the same way as presented in the previous section. Their detailed information is available in LSTC (2007a). These six curve-functions are tested as well and proved to be responsive. In this thesis, it is assumed that the ship moves towards the ice at a constant velocity before the impact takes place. The impact lasts for a short period of time, and the change of velocity is not significant. Including drag will require thrust to be modeled as well, which makes the analysis unnecessarily complicated. Therefore, drag is ignored.

DYNA also provides users with six functions that report accelerations in 6 DOF. They are ACCX, ACCY, ACCZ, WDTX, WDTY, and WDTZ (LSTC 2007a). In each DOF, the added mass effect can be theoretically modeled by defining a force as:

$$F = -a \cdot \Delta m \quad \text{Equation 5-4}$$

where a is the acceleration of the CG of the body given by user-defined-curve-functions and Δm is the added mass, and the minus sign means the force is in the opposite direction of the acceleration.

Both Popov's original model (Popov et al. 1967) and DDePS suggest that the added mass effect is very important in determining the ship-ice contact force. However, unfortunately, the added mass effect cannot be included in this thesis due to a bug associated with the acceleration curve-functions in DYNA. When the acceleration curve-functions are present

in the model, DYNA is not able to convert external node numbers to sequential internal node numbers. External nodes are nodes added by users to define the CG of the body and the local coordinate system (such as node 138003, node 138004 and node 138005 in Section 5.1.2). Internal nodes are the ones created by DYNA when it generates the mesh. Discussions and efforts have been made with other DYNA's users and DYNA's technical support to solve this issue (Kennedy, 2012). A workaround of manually numbering node numbers has been suggested, but it still cannot report translational accelerations and gives different rotational accelerations when solving the same model using different releases of DYNA. The author has been advised by DYNA's technical support that a new version is available and it may or may not have this issue resolved (Kennedy, personal communication).

5.2 Mass Reduction Coefficient

The mass reduction coefficient needs to be addressed before discussing the ship-ice contact force. It is one of the key parameters in determining the ship-ice contact force as mentioned in Section 2.1.2. It was originally applied to the ship-ice collision analysis by Popov et al. (1967). Its detailed derivation is available in Daley (2000) and Kendrick et al. (2000b). This subsection investigates if DYNA and Popov's original model have the same estimation on the mass reduction coefficient. Results from DYNA simulations are compared with calculations using the DDePS program.

5.2.1 Simulation Setup

In the solution using DYNA, the dimensions of the ship and ice are the same as in Section 3.1.1. The ship and ice are modeled as rigid since the deformation is not the concern. The material densities are the same as those in Table 3-2 and Table 3-3. Element choices are the same as in Table 3-4. Both the ship and ice are modeled as free bodies. The loading conditions in DDePS and in DYNA are the same to ensure comparable results. Loads are applied to ship and ice as if there was a collision. A quick contact simulation determines one node on the ship bow and another node on the ice as the contact location. A local coordinate system is constructed at the possible contact point on the ship bow. Its x-y plane lies in the ship bow plate, and its z-direction coincides with the normal direction of the bow plate (see Figure 5-3). This local coordinate system is the reference for defining the loading direction. Then a force is applied on the ship bow in the $-z$ -direction of the local coordinate system. Another force with the same magnitude is applied on the ice (node 49824 in Figure 5-4) in the z-direction of the local coordinate system in a separate analysis. The magnitude of the force equated the estimation by the DDePS for the same collision case. Restoring forces and added mass terms are not included in the analysis so it is a “dry” collision.

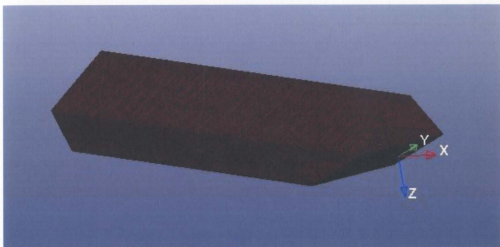


Figure 5-3: Normal Direction of the Contact Surface

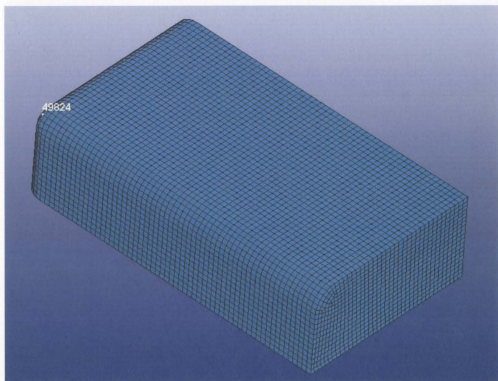


Figure 5-4: Contact Location on the Ice

5.2.2 Results

Accelerations in the x-, y-, and z-directions of the two bodies are recorded in DYNA's outputs. They are mapped back to the normal direction defined. The mass reduction coefficient is calculated as:

$$C_o = \frac{m}{\frac{F}{a_{normal}}} \quad \text{Equation 5-5}$$

where m is the mass of the body (the ship or ice), a_{normal} is the acceleration of the contact point in the normal direction of the contact surface, and F is the contact force. DDePS and DYNA have different estimations on radii of gyration as shown in Table 5-2, hence different mass moments of inertia. For the radii of gyration of the ship, the discrepancy lies in the different mass distributions of the geometric model. In the DYNA solution, the ship is a shell, while in the DDePS solution, the ship is considered as a solid body. For the radii of gyration of the ice, the two solutions give very similar estimations of r_x and r_y . However, they indicate very different values for r_z since DDePS's estimation is based on empirical values.

These two approaches also predict different added mass coefficients as discussed in Section 4.4. Various combinations of added mass coefficients and radii of gyration are input into DDePS to calculate the mass reduction coefficient. Results are presented in Table 5-3 along with DYNA's estimations. Note that for the same collision case, the contact force will increase as the mass reduction coefficient decreases. DDePS ① and the DYNA solution share the same condition, but DDePS ① gives higher estimations for the

C_D . Comparing DDePS ② and DDePS ① indicates that added mass decreases the mass reduction coefficient, which will consequently increase the effective mass and contact force. A comparison of DDePS ① and DDePS ③ suggests that radii of gyration of the bodies play an important role in determining the C_D . Radii of gyration given by DYNA and DDePS are different. To minimize this difference's influence, calculation of the contact force in DDePS will adopt the radii of gyration given by DYNA when comparing these two approaches. Comparing DDePS ③ and DDePS ④ also shows that added mass terms significantly reduce the C_D , and it implies that DDePS ④ will predict a much higher contact force than DDePS ③. The DDePS ⑤ gives smaller values compared to DDePS ② because the original DDePS model gives higher estimations for the added mass coefficients as discussed in Section 4.4.

Table 5-2: Radii of Gyration Estimated by DYNA and DDePS

	Ship		Ice	
	DYNA	DDePS	DYNA	DDePS
$r_x(m)$	5.1	3.8	4.5	4.6
$r_y(m)$	18.1	15.1	2.7	2.2
$r_z(m)$	18.4	16.5	5.0	2.1

Table 5-3: Mass Reduction Coefficients C_a

Solution	Description	Ship	Ice
DYNA	No added mass terms	2.73	2.27
DDePS①	Using DYNA's radii of gyration, but NO added mass terms	3.51	3.22
DDePS②	Using DYNA's radii of gyration & added mass terms	3.08	2.69
DDePS③	Using original DDePS' radii of gyration, NO added mass terms	4.38	4.86
DDePS④	Using original DDePS' radii of gyration & added mass terms	2.67	2.56
DDePS⑤	Using DYNA's radii of gyration & DDePS' added mass terms	2.16	1.84

It is apparent that DDePS and DYNA have different estimations for the added mass reduction effect. There are several reasons which may contribute to this discrepancy. First of all, the cross moments of inertia (I_{xy} , I_{yz} and I_{zx}) are ignored in DDePS but included in DYNA. Besides, DDePS assumes that moment arms of the body do not change during the contact, while this is not true in the DYNA solution. Moreover, in DDePS and Popov's model, it is assumed that the collision occurs in an instant time period, and the body rotates around its CG. In the DYNA model, although the impulse load is applied, the effect of force lasts slightly longer, and the rotational center of the body changes over time. The difference in the mass reduction coefficient should be taken into account when comparing the contact forces estimated using DDePS and DYNA.

5.3 Simulation Setup

This section presents the DYNA model for evaluating the global ship-ice contact force. Results are discussed in Section 5.4.

5.3.1 Geometric Model

The geometric model is the same as the one in Section 3.1.1.

5.3.2 Material Models

The material model for the ship is the same as the one in Section 3.1.2 (see Table 3-2).

The modified crushable foam ice model C from Section 3.2.4 is utilized to model the ice block. Its material properties are available in Table 3-8 and Table 3-11.

5.3.3 Element Choices

Element choices are same as those in Section 3.1.3 (see Table 3-4).

5.3.4 Boundary and initial conditions

In all simulations, the ship is modeled as a free body. For the collision with a finite ice mass, the ice is treated as a free body as well. For the collision involving an infinite ice, the ice is fixed on two sides as shown in Figure 3-6 to imitate an infinite mass of the ice.

In each case, the ship starts moving forward at a different initial speed. The ice is crushed and deforming as the contact proceeds. The ship-ice contact ceases when they bounce off each other. The ship's initial speed is 3m/s in the mesh convergence study.

5.3.5 Loading Conditions and Damping

The model does not include gravity or water, hence no net buoyancy. This could be interpreted as gravity equals buoyancy, i.e., each body is initially “floating” at the neutral buoyancy position. Restoring forces are applied following the instruction in Section 5.1.2. Since there are no heave, roll and pitch displacements prior to the collision, user-defined-curve-functions are applying zero forces to the floating bodies. Once the collision takes place, the ship-ice contact force begins to “push” the ship and ice to move in all 6 DOF. Heave, roll and pitch displacements then result in non-zero restoring forces. Drag and forces associated with the added mass are not included in the analysis as discussed previously. Load definitions are summarized in Table 5-4. There is no load definition on the infinite ice since it will not have any global motion. Damping is applied. The added mass terms are included in the calculation of damping coefficients.

Table 5-4: Load Definitions on the Ship and Ice

Motion	Load Definition on the Ship	Load Definition on the Ice
Heave	-6,828,219*DZ(904333)	-4,538,321*DZ(138003)
Roll	-35,247,518*AX(904333)	-23,631,412* AX(138003)
Pitch	-1,813,659,196*AY(904333)	-6,661,882*AY(138003)

Note: Node 90433 is the CG of the ship. Node 138003 is the CG of the ice.

5.3.6 Mesh Convergence

Mesh convergence studies are conducted for both the ship glancing with finite and infinite ice cases. Time histories of the contact forces from simulations using various

element sizes are compared in Figure 5-5 and Figure 5-6. Note that the contact starts at a different time instant as the mesh density changes. Measuring the distance between the ship and ice suggests that the contact should initiate at about 1.5 seconds. Simulations using elements no larger than 0.24m give similar results. Reducing the element size from 0.12m to 0.1m barely changes the results. However, analyses using 0.1m element take a significantly longer time to solve as shown in Table 5-5. Note that 0.12m is also an appropriate size for meshing the ship structure assuming non-uniform mesh is used. Therefore, 0.12m is considered as the optimal element size for modeling the ship-ice contact force.

Table 5-5: Computation Time of Simulations using Various Element Sizes

Element Size	0.35m	0.24m	0.2m	0.15m	0.12m	0.1m
Finite Ice Case	40sec	1.5min	4min	21min	1.4hr	6hr
Infinite Ice Case	37sec	2min	5min	27min	1.8hr	7.8min
No. of Compute Nodes	4	4	4	4	4	4

Note: All simulations are solved on STePS2 Cluster (see Appendix A)

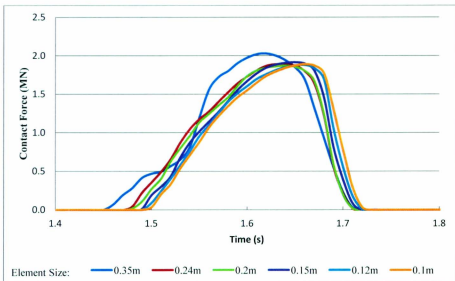


Figure 5-5: Mesh Convergence – Ship Glancing with Finite Ice

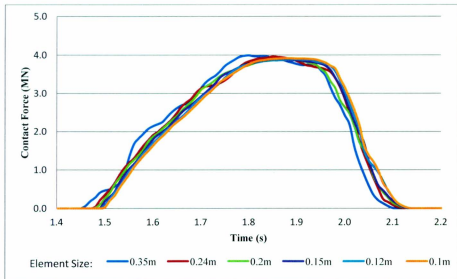


Figure 5-6: Mesh Convergence – Ship Glancing with Infinite Ice

5.4 Ship-Ice Contact Force

Ship-ice glancing scenarios at various ship speeds are simulated using the numerical model presented in the previous section. Results are compared with the calculation using the DDePS program. For the finite ice case, the deformation in the ice is small and the shape of the contact area is similar to Scenario 2C in DDePS. For the infinite ice case, the deformation is much larger and the shape of the contact area is similar to Scenario 2B in DDePS. As discussed in Section 5.2.2, DYNA and DDePS give different values of the radii of gyration of a body. To minimize this difference's influence on the contact force, all calculations of the contact force using DDePS adopt the radii of gyration given by DYNA.

5.4.1 "Dry" Collision Cases

The term "Dry" collision means any effect related to water is excluded in the analysis. Restoring forces modeled using user-defined-curve-functions and damping are removed from the DYNA analysis. In the DDePS calculation, all the added mass values are set at zero. As discussed in the previous section, the mass reduction coefficient C_o must be taken into consideration when evaluating the contact force. The original C_o derived by Popov et al. (1967) and the ones estimated by DYNA are input into DDePS to evaluate the contact force. Contact forces of various "dry" collisions are compared in Table 5-6 (finite ice) and Table 5-7 (infinite ice). Note that:

- DDePS ① solution directly applies the C_o given by DYNA rather than following the derivation by Popov et al. (1967).

- DDePS ② solution calculates the C_o following Popov's original derivation with the radii of gyration given by DYNA.
- DDePS ① and the DYNA solutions are based on the same mass reduction coefficients. DDePS ② has larger mass reduction coefficients.

Table 5-6: Maximum Contact Force (Finite Ice, Dry Collision)

Ship Speed (<i>m/s</i>)	2	3	4	5
DYNA (<i>MN</i>)	1.26	1.86	2.44	3.04
DDePS ①(<i>MN</i>)	1.39	2.03	2.68	3.31
DDePS ② (<i>MN</i>)	1.19	1.74	2.28	2.82

Table 5-7: Maximum Contact Force (Infinite Ice, Dry Collision)

Ship Speed (<i>m/s</i>)	2	3	4	5
DYNA (<i>MN</i>)	2.62	3.83	5.22	6.71
DDePS ①(<i>MN</i>)	2.37	3.78	5.25	6.79
DDePS ② (<i>MN</i>)	2.09	3.32	4.62	5.98

It is clear that the mass reduction coefficient has a significant influence on the contact force. DYNA and DDePS ① have the same mass reduction coefficients and show very good agreement. Especially in the case of the infinite ice (large deformation in the ice), the two solutions give identical results. In the case of the finite ice (small deformation in

the ice), the difference in the results are slightly larger due to the ice material model. The pressure-area curve of the ice material model in DDePS strictly follows the $P = A^{-0.1}$ relationship. In the DYNA solution, the pressure-area relationship of the ice model agrees very well with the curve $P = A^{-0.1}$ for large deformations, but does not perfectly fit it when the deformation is small as discussed in Section 4.4. Compared to its mathematical approximation, the ice model actually exerts higher pressures over small contact areas. Overall, these two solutions give similar estimations of the ship-ice contact force.

5.4.2 “Wet” Collision Cases

“Wet” collision means that restoring forces and damping are included in the DYNA solution, while added mass is considered in the DDePS solution. There is no restoring force or damping in the DDePS solution. Results are listed in Table 5-8 (finite ice) and Table 5-9 (infinite ice). Note that:

- Only the ship's C_o matters here since the ice is modeled as infinitely large.
- In all the DDePS solutions, the calculation of C_o follows Popov's derivation (Popov et.al 1967) with radii of gyration given by DYNA.
- The solution DDePS ① uses Popov's original added mass terms. It has the smallest C_o among the three solutions.
- The solution DDePS ② uses DYNA's added mass terms (see Table 4-10). It has the largest C_o , but its value is only slightly larger than the C_o given in the DYNA solution.

Table 5-8: Maximum Contact Force (Finite Ice, Wet Collision)

Ship Speed (<i>m/s</i>)	2	3	4	5
DYNA (<i>MN</i>)	1.27	1.88	2.47	3.06
DDePS ① (<i>MN</i>)	1.53	2.25	2.96	3.66
DDePS ② (<i>MN</i>)	1.28	1.89	2.38	2.95

Table 5-9: Maximum Contact Force (Infinite Ice, Wet Collision)

Ship Speed (<i>m/s</i>)	2	3	4	5
DYNA (<i>MN</i>)	2.65	3.89	5.30	6.89
DDePS ① (<i>MN</i>)	2.75	4.38	6.10	7.88
DDePS ② (<i>MN</i>)	2.25	3.58	4.99	6.45

In the DYNA model, added mass terms are not included, but in the DDePS solution, added mass terms are involved in computing the mass reduction coefficient and consequently have a direct influence on the contact force. These three solutions should not give similar estimations for the contact force because of the different mass reduction coefficients. The agreement of DDePS ① and DYNA is due to the approximation in the ice material model as discussed in the previous section. DDePS ② has a slightly larger C_0 than the DYNA solution and thus predicts a similar but smaller contact force in most cases. DDePS ① has the smallest mass reduction coefficient and therefore gives the largest contact force. The DDePS ② solution features the largest mass reduction

coefficients and suggests the smallest contact forces. The added mass is another factor that contributes to the difference in the results.

5.4.3 “Dry” vs. “Wet”

In the DYNA model, the ship and ice bounce off each other immediately after the contact in the “dry” collision, while restoring forces and damping causes the two bodies to stay in contact in the “wet” collision. Therefore, the contact force in a “wet collision” is expected to be larger and last longer than that in a “dry” collision. It is verified by comparing the maximum contact forces in Table 5-10 and Table 5-11. The difference in the infinite ice case is much more obvious than that of the finite ice case. However, this increase in the contact force is not significant compared to its maximum value. This means that restoring forces are not important in determining the contact force of the first impact. This agrees with Popov’s original assumption.

In the DDePS solution, the ship and ice are always assumed to bounce off each other in both the “dry” and “wet” collisions. The difference is that, in the “wet” collision, added mass terms are directly applied to the calculation of the mass reduction coefficient and significantly reduces the mass reduction coefficient, i.e., increase the effective mass. This consequently increases the contact force. Therefore, the increase in the contact force is more significant as the condition changes from “wet” to “dry” in the DDePS solution.

The change of the contact force from the “dry” to “wet” collision is demonstrated in Table 5-10 and Table 5-11. In the DDePS solution, results are from the analyses where radii of gyration, and added mass coefficients given by DYNA are used to calculate the contact force. This practice is done for minimizing the difference in the inputs of the two solutions.

Table 5-10: Dry vs. Wet – Maximum Contact Force, Finite Ice

Ship Speed (<i>m/s</i>)	DYNA (<i>MN</i>)			DDePS (<i>MN</i>)		
	Dry	Wet	Increase	Dry	Wet	Increase
2	1.26	1.27	0.8%	1.19	1.28	7.6%
3	1.86	1.88	1.1%	1.74	1.89	8.6%
4	2.44	2.47	1.2%	2.28	2.38	4.4%
5	3.04	3.06	0.7%	2.82	2.95	4.6%

Table 5-11: Dry vs. Wet – Maximum Contact Force, Infinite Ice

Ship Speed (<i>m/s</i>)	DYNA (<i>MN</i>)			DDePS (<i>MN</i>)		
	Dry	Wet	Increase	Dry	Wet	Increase
2	2.62	2.65	1.2%	2.09	2.25	7.7%
3	3.83	3.89	1.6%	3.32	3.58	7.8%
4	5.22	5.30	1.5%	4.62	4.99	8.0%
5	6.71	6.89	2.7%	5.98	6.45	7.9%

In the DYNA solution, the difference in the time histories of the contact forces is much more dramatic. Taking the case where the ship speed is $5m/s$ for example, time-histories of the contact forces are compared in Figure 5-7 (finite ice) and Table 5-11 (infinite ice). Besides a higher maximum contact force, the “wet” collision also predicts a second contact and even a third contact. Note that the DDePS program is only capable of estimating the first impact.

In conclusion, restoring forces modeled by user-defined-curve-functions have a small influence on the contact force of the first impact, but are very important in simulating the bodies’ motions after the first impact as well as the second impact. This suggests that the contact force is dictated by the contact speed, mass, and the material strength of the contacting bodies. Another important aspect is that the solution using user-defined-curve-functions only takes about one hour to solve, which is significantly more efficient than the ALE method.

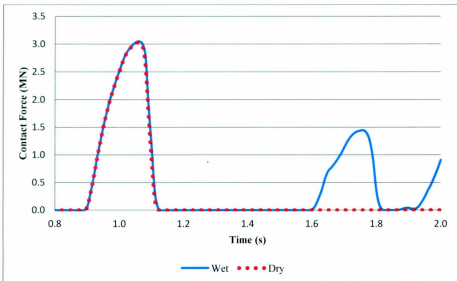


Figure 5-7: Comparison of the Contact Force – Dry vs. Wet (Finite Ice)

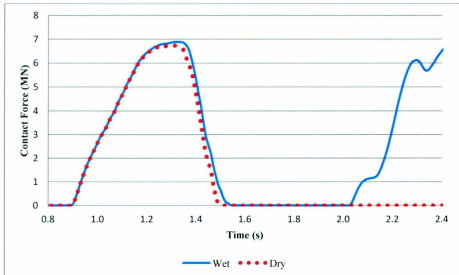


Figure 5-8: Comparison of the Contact Force – Dry vs. Wet (Infinite Ice)

5.5 Summary

This chapter explains the implementation of user-defined-curve-functions to model restoring forces. Theoretically, forces related to added mass and drag can be modeled in the same way. However, forces related to added mass are not included due to a problem in DYNA. Drag is ignored because it is not necessary in this analysis. This practice greatly reduces computation cost compared to the ALE method. The mass reduction coefficients estimated by DYNA and DDePS are compared and shown to be important in determining the contact force.

When the same mass reduction coefficients are applied, DYNA and DDePS give identical estimations for the contact force. This agreement is more obvious in the infinite ice case than in the finite ice case. For the finite ice cases, the present DYNA model gives higher estimations for the contact forces. This is because the ice model in the DYNA solution does not strictly follow the form $P = A^{-0.1}$. As discussed in Section 4.4, compared to the mathematical approximation, the ice model actually exerts higher pressures over small contact areas. Overall, these two approaches have demonstrated a good agreement.

Restoring forces modeled by user-defined-curve-functions have a small influence on the maximum contact force of the first impact, but are very important in simulating the motions of the ship and ice as well as the second impact. This suggests that the contact force is dictated by the contact speed, mass, and the material strength of the contacting bodies. Another important aspect is that the solution using user-defined-curve-functions

only takes about one hour to solve, which is significantly more efficient than the ALE method.

Chapter 6 Ship's Structural Response

The previous chapters have addressed modeling the ice material, the water domain, and the ship-ice contact model. This chapter proposes the final model by combining all the previous work together and incorporating the ship's local structural response. However, this chapter does not intend to conduct a comprehensive or sophisticated structural analysis. Its purpose is to give a simple demonstration of how to use the final model to perform structural analysis. It serves more as a general guideline rather than validating any results. Readers can follow the guidance given in this chapter to build more elaborate models for more comprehensive and detailed structural analysis.

6.1 Ship Structural Design

The ship hull used in previous chapters is ice-strengthened with internal structures in accordance with the URI and DNV specifications. Since the ship ice contact will occur at the ship bow, the structural design is only conducted for the bow area. The bow region, including its structural members, will be modeled using elastic-plastic material, while the rest of the ship is modeled as rigid. The ship structural design presented in this chapter is not for ship-building purposes. This practice aims to give a simple structural model to proceed with the analysis of the ship structural response. If the ship's structural model is available, it can be directly input into DYNA to generate the geometric model and the mesh.

6.1.1 Main Frames

The design of the main web frames complies with Section I2 of the URI (IACS 2010), which utilizes the plastic strength of the structural members. Derivation of the formulations for the framing design in the URI can be found in Daley (2002), and Kendrick et al. (2000b). The URI divides the ship hull into several regions. A different level of ice load is expected in each region. The hull is divided into four regions in the longitudinal direction: bow, bow intermediate, midbody, and stern. The bow intermediate, midbody, and stern are then vertically divided into sub-regions: icebelt, lower, and bottom. The extent of each region is shown in Table 6-1 and Figure 6-1.

Table 6-1: Hull Area Extents (IACS 2010)

Region/Area	Notation
Bow	B
Bow Intermediate Icebelt	Bli
Bow Intermediate Lower	Bll
Bow Intermediate Bottom	Blb
Midbody Icebelt	Mi
Midbody Lower	Ml
Midbody Bottom	Mb
Stern Icebelt	Si
Stern Lower	Sl
Stern Bottom	Sb

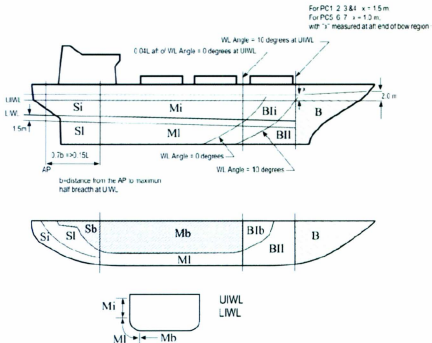


Figure 6-1: Hull Area Extents (IACS 2010)

The ship is chosen as a Polar Class-4 ship. All necessary geometric information for the ship's structural design is listed in Table 3-1. The main frames are transversely arranged on the ship hull. Their dimensions are listed in Table 6-2 in Section 6.1.5. A snapshot of the 3D model (in Rhinoceros®) of the main frames is illustrated in Figure 6-2. The gaps between the main web frames are occupied by deep web frames and bulkheads.

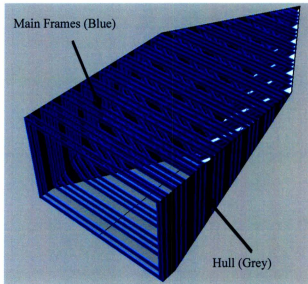


Figure 6-2: Main Frames and the Hull

6.1.2 Load Carrying Stringers

The URI does not address the scantling requirements on load carrying stringers. Their scantlings are determined following the DNV's specifications titled Ships for Navigation in Ice (2011). This limits the strength of load carrying stringers to the elastic range. Load-carrying stringers are oriented longitudinally on the ship hull. Detailed scantlings of the load carrying stringers are listed in Table 6-2 in Section 6.1.5. The 3D models (in Rhinoceros®) of the load carrying stringers are illustrated in Figure 6-3.

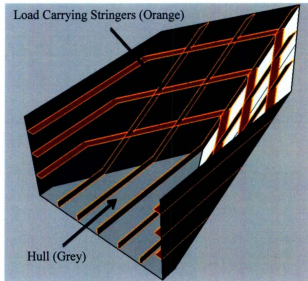


Figure 6-3: Load Carrying Stringers and the Hull

6.1.3 Deep Web Frames

The URI does not address the scantling requirements for deep web frames. Their scantlings are determined following the DNV's specifications titled *Ships for Navigation in Ice* (2011) as well. This also limits the strength of deep web frames to the elastic range. Deep web frames are oriented transversely on the ship hull. Detailed scantlings of the deep web frames are listed in Table 6-2 in Section 6.1.5. The 3D models (in Rhinoceros®) of the deep web frames are illustrated in Figure 6-4.

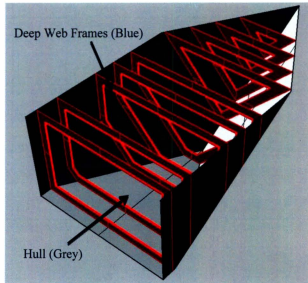


Figure 6-4: Deep Web Frames and the Hull

6.1.4 Bulkheads

The design of the bulkheads does not follow any specifications. A bulkhead is placed on the hull every 10 main frames. The thickness of the bulkhead is 30mm. Each bulkhead is stiffened with flat bars that are 300mm in height and 30mm in thickness. The 3D model (in Rhinoceros®) of the bulkheads is illustrated in Figure 6-5.

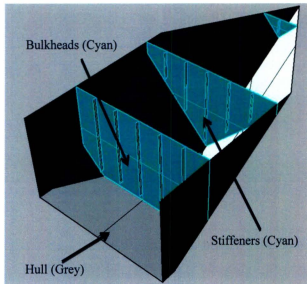


Figure 6-5: Bulkheads including Stiffeners, and the Hull

6.1.5 Summary

The scantlings of the structural members on the bow are summarized in Table 6-2. The 3D model (in DYNA) of the bow region with internal structural members is illustrated in Figure 6-6. It must be emphasized that the structural design is not for ship building purposes. This practice only aims to generate a simple geometric model for the structural analysis.

Table 6-2: Scantlings of Structural Members in the Bow Region

Item	Main Frame	Load Carrying Stringer	Deep Web Frame
Orientation	Transverse	Longitudinal	Transverse
Spacing, <i>m</i>	0.5	2	2
Span, <i>m</i>	2	2	2
Hull Plate Thickness, <i>mm</i>	30	30	30
Web Height, <i>mm</i>	300	600	700
Web Thickness, <i>mm</i>	22	30	30
Flange Width, <i>mm</i>	0	0	120
Flange Thickness, <i>mm</i>	0	0	30

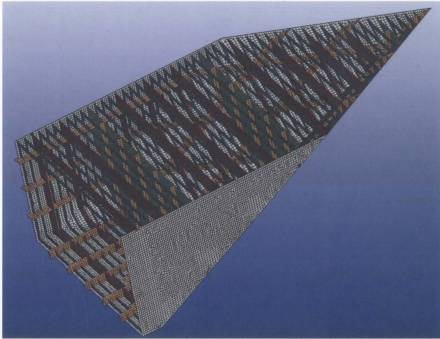


Figure 6-6: Bow Region with Internal Structural Members

6.2 Simulation Setup

A simulation of a ship-ice glancing scenario from Chapter 5 is repeated with the ship modeled using a combination of elastic-plastic and rigid materials to include its structural response. A simple evaluation of the local structural response of the ship bow is given as an example of how to use the proposed model.

6.2.1 Geometric Model

The ship hull and the ice block are the same as in previous chapters. Their detailed information is available in Table 3-1. The ship hull is strengthened with structural members as discussed in the previous section.

6.2.2 Material Model

The ship is modeled using a combination of rigid and non-rigid materials to save computation cost. The bow region and its internal structural members are modeled using the elastic-plastic material. Its properties are shown in Table 6-3. The rest of the ship is treated as rigid. Properties of the rigid material are the same as in Section 3.1.2 (see Table 3-2).

Table 6-3: Material Parameters for the Non-Rigid Part of the Ship

Card ID	MAT_PIECEWISE_LINEAR_PLASTICITY (MAT_024)			
Density	Young's Modulus	Poisson's Ratio	Yield Stress	Tangent Modulus
7850kg/m ³	200GPa	0.3	350MPa	1GPa

The ice block is modeled using a combination of rigid and non-rigid materials as well. The modified crushable foam ice model C from Section 3.2.4 is utilized to model the deformable part. Its material properties are available in Table 3-8 and Table 3-11. Material parameters of the rigid part are listed in Table 6-4. The 3D model is shown in Figure 6-7.

Table 6-4: Material Parameters of the Rigid Part of the Ice

Card ID	MAT_RIGID (MAT_020)		
Material Type	Density	Young's Modulus	Poisson's Ratio
Rigid	900kg/m ³	5GPa	0.03

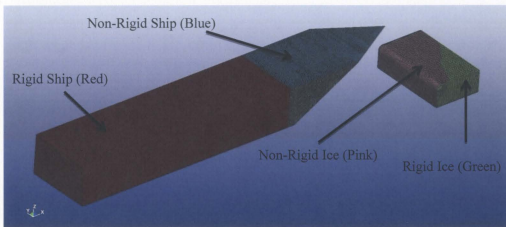


Figure 6-7: Rigid and Non-Rigid Ship and Ice

As shown in Figure 6-7, the non-rigid portions of the ship and ice are not small compared to the overall dimensions of the ship and ice. In a more elaborate analysis, users can model larger portions of the geometric models as rigid to save more computation cost.

6.2.3 Element Choices

Element choices are shown in Table 6-5. The Belytschko-Tsay formulation is recommended for structural analysis (Quinton 2009). An average element size of 0.15m is used for the mesh without conducting a mesh convergence study. This is because the present chapter only intends to give a simple demonstration of structural analysis rather than giving an accurate answer. In a more elaborate analysis, not only the element size should be carefully chosen, but also a mesh with non-uniformly sized elements should be used. Areas far away from the possible contact region can be treated with very coarse mesh and the contact region on the ship and ice should be meshed with local refinements.

Table 6-5: Element Choices

Part	Element Type	Formulation Option	Ambient Type
Ship	Shell	2 (Belytschko-Tsay)	N/A
Ice	Solid	1 (Default)	0

6.2.4 Boundary and initial conditions

This is a simulation of a glancing scenario between the ship and an infinite ice. Therefore the ship is modeled as a free body. The ice is fixed on two sides as shown in Figure 3-6 to mimic an infinite mass. The ship starts moving forward at an initial speed of $4m/s$. The ice is crushed and deforms as the contact proceeds. The ship's bow region displays an elastic-plastic structural response as well. The ship-ice contact ceases when the two bodies bounce off each other.

6.2.5 Loading Conditions and Damping

The model does not include gravity or water; hence there is no net buoyancy. This could also be interpreted as gravity equals buoyancy, i.e., each body is initially "floating" at the neutral buoyancy position. Restoring forces are applied following the method discussed in Chapter 5. Extra mass is assigned uniformly to all the nodes on the ship so that it weighs the same as in previous chapters. However, the CG of the ship is different from that in the previous chapters due to a different mass distribution. This also changes the mass moments of inertia of the ship, and consequently changes the load definition. The updated load definitions are summarized in Table 6-6.

Table 6-6: Load Definition on the Ship

Motion	Load Definition
Heave	-6,828,219*DZ(904333)
Roll	-35,247,518*AX(904333)
Pitch	-1,813,659,196*AY(904333)

6.3 Ship Structural Response

The model is solved using the STePS2 cluster with 4 compute nodes (32 cores). The computation time is about 36 hours, which is reasonably low considering the amount of plots generated in the output. This computation cost can be significantly reduced by modeling a larger portion of the model as rigid, using a non-uniform mesh, and requesting fewer plots in the output. This section gives a short and simple discussion of the ship's structural response in terms of the contact load, Von Mises stress, and the pressure-deflection curve.

6.3.1 Contact Force and Pressure

The time history of the resultant ship-ice contact force is illustrated in Figure 6-8. The red line is the contact force of the same collision simulation except that the ship is modeled as rigid. The value of the contact force significantly decreases when modeling the ship as deformable rather than rigid. It is because the deformation in the ship structure absorbs a large amount of energy. The time history of the estimated average contact pressure is shown in Figure 6-9. It suggests that average pressure is not high enough to cause yield.

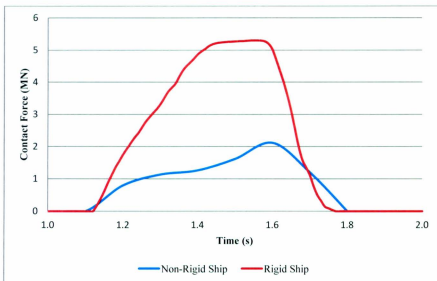


Figure 6-8: Comparison of the Contact Force: Rigid Ship vs Non-Rigid Ship

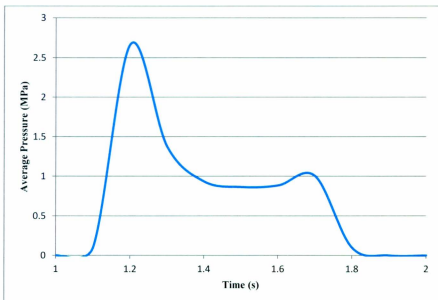


Figure 6-9: Time History of the Average Pressure

6.3.2 Von Mises Stress

Von Mises stress is one of the most important criteria in structural engineering analysis. In this simulation, the ship-ice contact force is a moving load as the ice moves along the ship hull. The pressure distribution on the ship bow is characterized with high pressure zones within lower pressure zones, which causes some elements develop much higher effective stress than their neighboring elements. This phenomenon is shown in Figure 6-10 and Figure 6-11. As mentioned earlier, the average contact pressure is not high enough to cause structural members to yield. This is confirmed by the result that most members show a pure elastic response as shown in Figure 6-11. However, the high concentration of pressure still causes a couple of sections on the main frames to yield and move to the plastic range as shown in Figure 6-10. The analysis of the structural response focuses on the main frame members with elements that display an elastic-plastic behavior. Figure 6-12 illustrates the time history of the Von Mises stress of the element that is under investigation. The same element's effective plastic strain is shown in Figure 6-13. It is apparent that the plastic strain starts to develop as the effective stress exceeds the specified yield stress of 355 *MPA*. This shows that the plastic capacity of the main frame members have been utilized as designed.

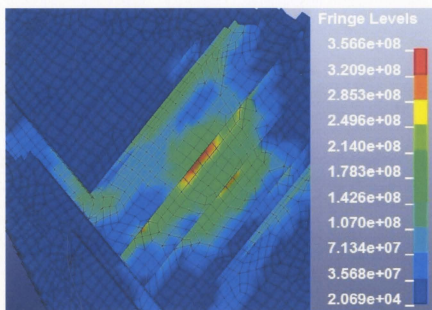


Figure 6-10: A Typical Von Mises Stress Distribution on the Main Frame

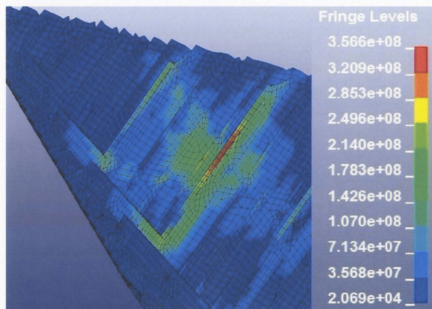


Figure 6-11: A Typical Von Mises Stress Distribution on the Deep Web Frame

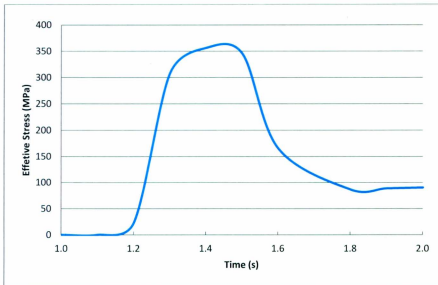


Figure 6-12: Time History of the Effective Stress

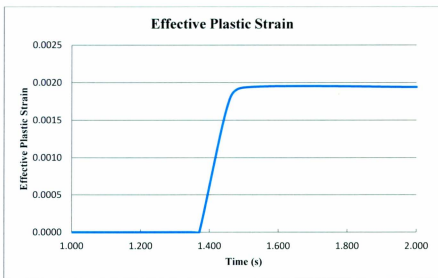


Figure 6-13: Time History of the Effective Plastic Strain

6.3.3 Pressure-Deflection Curve

The last task is analyzing the pressure-deflection relationship of the main frame members. This analysis is fairly easy to conduct for the static FEA where the structure is fixed on the boundary, and the ship-ice contact is simply replaced by a point load or a patch load as the ice load. This setup implies that the deflection of the structure is essentially the displacement of the node (or nodes) on the mesh, which is available in DYNA output. The value of the load/pressure that causes the deflection can be accurately determined since it is directly defined by the user.

In this simulation, the ship-ice contact force is a moving load, and the ship is free to move in 6 DOF. This makes it impossible to accurately analyze the pressure-deflection curve of the structure. As mentioned earlier, the average contact pressure is not high enough to cause yield, therefore the analysis of the pressure-deflection relationship focuses on the high pressure zone where elements show an elastic-plastic behavior. Values of the load given by DYNA include the load on the member under investigation, and the loads on other members. A careful examination of the data suggests that elements that eventually yield are subject to the moving ice load roughly from 1.2 seconds to 1.6 seconds. Values of the pressure on the contact interface are examined. Values of the corresponding loading areas are manually measured in the DYNA output. The deflection is roughly calculated by subtracting the displacement due to the global motion from the total displacement given by DYNA, which is an approximation to the actual deflection.

Combining all the information above gives a rough estimation of the pressure-deflection curve, which is shown in Figure 6-14.

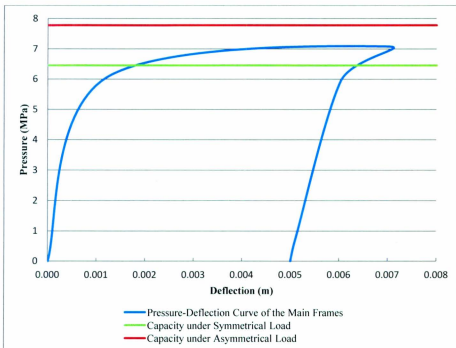


Figure 6-14: Pressure –Deflection Curve of the Main Frame Member

In the simulation, the loading condition on the main frame changes from asymmetrical to symmetrical, and then back to asymmetrical as the ice moves along the ship bow. The capacities under asymmetrical load and symmetrical load are plotted as well. They are calculated using the equations proposed by Kendrick et al. (2000) and Daley (2002). Their values are higher than what is suggested by the pressure-deflection curve. It is because the information for generating this pressure-deflection plot is obtained via

estimation and manually measured from the DYNA output, which inevitably introduces errors to the plot. However, it is very clear that the structural response features an extended plastic region. This is because the main frames are designed as members on a PC-4 ship, while the ice material model complies with the one specified for PC-3. It is also apparent that the plastic strength of the structural members is utilized to resist the ice load as designed. The structural members have developed plastic strain, residual deflection, and post-yield residual stress.

6.4 Summary

This chapter proposes the final model by combining all the previous work together and incorporating the ship's local structural response. However, this chapter does not intend to give a full treatment to the structural analysis. It is purely for giving a general example of how to use the proposed model to carry out structural analysis of the ship under ice impacts. Users can follow the direction given in this chapter to build more elaborate models and obtain more comprehensive and sophisticated results.

As shown in this chapter, the model developed in this thesis is capable of giving the global motions of the ship and ice, the global ship ice contact load, ice failure, and ship's structural response in one package. The computation time of the proposed model is reasonably low and can be further reduced by modeling a larger portion of the model as rigid, and using a non-uniform mesh. A mesh convergence study is not conducted for this

simulation. A more refined mesh on the contact region and local structural is necessary for a more accurate structural analysis.

Chapter 7 Conclusions and Recommendations

The goal of this study is to define a procedure of analyzing ship-ice collision using the commercial FEA software DYNA. The final product is an efficient FEA solution that is capable of evaluating the hydrodynamic forces, the global motions of the ship and ice, the contact force, ice failure, and the ship structural response in one efficient analysis. In order to achieve this goal, the work was completed as four subtopics as stated in Section 1.2. The conclusion for each subtopic has been discussed in the end of the corresponding chapter. The work is summarized and presented in this chapter with general conclusions.

7.1 Conclusions

First of all, three ice material models are proposed. They are the foundation of the present study. Their pressure-area curves have demonstrated good agreement with those specified in the URI. These ice material models have practical applications. They can also be further modified to serve different purposes.

Modeling water using the ALE method has been discussed. This study has shown that the ALE method is not practical when the model contains a very refined mesh constructed by a large number of elements. Moreover, the ALE method is not an ideal approach if the hydrodynamic effects are significant, due to the nature of the ALE method. However, the ALE method is useful if the analysis focuses on the low frequency global motions of the floating bodies as shown in several existing studies.

As an alternative to the ALE method, this research proposes to model the fluid effect user-defined-curve-functions in DYNA. The global ship-ice contact forces in various ship-ice glancing scenarios have been evaluated. The present solution agrees well with the DDePS solution when the same mass reduction coefficient is applied. This research simulates restoring forces using displacement springs rather than actually modeling water to improve efficiency. The restoring forces are shown to have small influence on the first impact force, but are important in estimating the second impact. This conclusion agrees with DDePS. Drag force is not necessary to be included in this type of simulations. On the other hand, the added mass effect should be considered. However, it is not present in the solution due to software problems. The ship-ice contact model proposed by this thesis is a very efficient solution for assessing the global ship-ice contact force.

In the last part of this thesis, the solution developed previously is extended to include the ship-structural response. The elastic-plastic behavior of the ship structural members is observed. The final solution gives the global motions of the ship and ice, the contact force, ice failure, and the ship structural local response in one package. The computation cost is fairly low and can be further reduced by modeling larger portions of the bodies as rigid. Overall, the initial goal of this thesis has been achieved.

7.2 Recommendations

Several questions have arisen during this research that prompt further research. The most important improvement that can be made is to include the added mass in the solution.

Modeling the added mass using user-defined-curve-functions is likely the most cost-effective method. It is necessary to determine why the curve-functions of accelerations behave inconsistently when solving the same model using different releases of DYNA. Personnel from LSTC have advised that the latest release of DYNA may have this issue resolved. If not, a workaround can be made by assigning extra mass to the ship and ice as the added mass. Users can customize the value of the added mass in each of the 6 DOF using the *PART_INERTIA card. If the new release can model the added mass as discussed in Section 5.1, the values of the added mass coefficients should be appropriately chosen. As discussed in this thesis, for a given floating body, the added mass effect under the instant impact load is different from that in the rotational and translational motions. DYNA is not the ideal tool for estimating the added mass due to its nature of calculating the fluid-structural interaction force. It is better to use CFD programs or experiments to perform this task. The latest version of DYNA has incorporated an incompressible flow solver. It does not require the usage of curve-functions and might be the most accurate solution for simulating the water domain where the ship-ice contact occurs.

Once the added mass issue is resolved, it is recommended to further assess its influence on the mass reduction coefficient via FEA using DYNA. The added mass can be easily incorporated into the model discussed in Section 5.1 using user-defined-curve-functions. DDePS suggests that the added mass significantly reduces the mass reduction coefficient, and consequently increases the effective mass and the contact force. It is desired to

investigate this phenomenon in DYNA. Another future work depending on the added mass is to simulate more ship-ice contact scenarios using the contact model proposed in Chapter 5. DDePS provides very quick solutions for more than 20 different ship-ice contact scenarios. All of them can be simulated by simply modifying the geometrical model in the contact model presented in Chapter 5. It is optimal to compare the results given by DYNA against the estimations by DDePS.

Another future work related to hydrodynamics is to apply drag force on the finite ice mass. Drag force can slow the ice from moving away from the ship and give a better estimation of the contact force. In other analyses, it might be necessary to apply drag force on the ship as well depending on the assumption related to the ship velocity.

Another recommended future work is to better measure the nominal contact area when its value is small. When developing ice material models, the nominal contact area derived from Rhinoceros® is not perfectly consistent with the actual nominal contact area in DYNA. Although this discrepancy has been reduced, it still hinders the accurate interpretation of the pressure-area curve of the ice material model. It is optimal to solve this problem to improve the present solution for analyzing the impact between a ship and a finite ice.

Another possible improvement concerns the ice material model. When developing ice material models, applying the theory of design of experiments will help with calibrating

material parameters and their combinations to yield desired results. In addition, modeling the ice using material models other than the crushable foam model should be further explored. It is recommended to start with the nonlinear elastic-plastic material model with the MAT_PIECEWISE_LINEAR_PLASTICITY card in DYNA. This material model gives users a large control over the material's stress-strain relationship.

During this research, numerical instability occurred when modeling ice blocks with sharp edges. When the element size is small, the contact involving sharp edges tends to introduce the negative volume problem in DYNA. This issue could be mitigated by properly introducing material erosion, or choosing a more robust material, such as the nonlinear elastic-plastic material.

This study does not investigate the size of the contact area when evaluating the ship-ice contact force given by DYNA's simulations. This should be included in future studies.

The mathematical approximation of the ice material is not very accurate for very small contact areas. Information of the exact contact area can help users to gain confidence in the results, and to better understand the possible difference in the DYNA solution and the DDePS solution.

The final finite element model proposed by this thesis can also be improved. First of all, a mesh convergence should be conducted. It is possible that the ship structural members should be meshed using smaller elements for a more accurate structural analysis. This should be a local refinement on the mesh to avoid significantly increasing the total

number of elements. Secondly, it is necessary to develop a method to more accurately measure the pressure and deflection for analyzing the pressure-deflection curve, which is very difficult to do when both the ship and ice are moving. It is much simpler to perform the pressure-deflection analysis on a local model of the ship structure. The section of the ship can be fixed on the boundaries, and the ship-ice impact can be replaced by a moving load on the structure. Another future work is to further reduce the computation cost. Using non-uniformly sized elements to generate the mesh can significantly reduce the total number of elements. Users can also try modeling larger partitions of the ship and ice as rigid to reduce the computation time, since the effect of the impact is highly localized.

Finally, DYNA is a very powerful and evolving FEA program with so many functions to be further explored. The author has experience with other commercial FEA software, and strongly believes that DYNA is the best available tool for addressing the ship-ice collision problem. Although this thesis does not provide answers to all the issues, it serves as the platform which further development can be built up on.

Chapter 8 Bibliography

- Daley, C.G., 1999, Energy Based Ice Collision Forces, Proceedings of the 15th International Conference on Port and Ocean Engineering under Arctic Conditions, POAC'99, Vol.2, pp. 687-696, Helsinki, Finland, August 23-27, 1999.
- Daley, C.G., 2000, IACS Unified Requirements for Polar Ships – Background Notes – Design Ice Loads, Prepared for IACS Ad-hoc Group on Polar Class Ships Transport Canada, 2000.
- Daley, C.G., Oblique Ice Collision Loads on Ships Based on Energy Methods, Ocean Eng Int 2001; 5(2): 67-72.
- Daley, C.G., 2002, Derivation of Plastic Framing Requirements for Polar Ships, Marine Structures 15 (2002) 543-559.
- Daley, C.G., 2004, A Study of the Process-Spatial Link in Ice Pressure-Area Relationships.
- Daley, C.G., 2007, Reanalysis of Ice Pressure-Area Relationships, Marine Technology, Vol. 44, No. 4, October 2007, pp. 234-244.

Daley, C.G., Kendrick, A., 2008, Direct Design of Large Ice Class Ships with emphasis on the Midbody Ice Belt, Proceedings of the 27th International Conference on Offshore Mechanics and Arctic Engineering OMAE2008 July 15-20, 2008, Estoril, Portugal. paper 2008-57846.

Daley, C., Kendrick, A., Yu, H., Noh, B-J., 2007, Structural Design of High Ice Class LNG Tankers, RINA Conference Design & Construction Of Vessels Operating In Low Temperature Environments 30 - 31 May 2007, RINA HQ, London, UK.

Daley, C.G., Liu, J., 2009a, DDePS for Ship and Infinite/Finite Ice Interaction, Report by BMT Fleet Technology Limited, submitted to Research & Product Development, American Bureau of Shipping, Jan, 2009.

Daley, C.G., Liu, J., 2010, Assessment of Ship Ice Loads in Pack Ice, International Conference and Exhibition on Performance of Ships and Structures in Ice, Anchorage, Alaska, USA September 20-23, Paper No ICETECH10-141, 2010.

Daley, C.G., Yu, H., 2009b, Assessment of Ice Loads on Stern Regions of Ice Class Ships, International Conference on Ship and Offshore Technology: Ice Class Ships, 28 - 29 September 2009, Busan, Korea.

Derradji-Aouat, A., 2003, Multi-Surface Failure Criterion for Saline ice in the Brittle Regime, cold Regions Science and Technology, vol. 36, pp. 47-70, 2003.

DNV, 2011, Ships for Navigation in Ice, Rules for Classification of Ships - Newbuildings - Special Service and Type - Additional Class

Frederking, R., 1998, The Pressure Area Relation in the Definition of Ice Forces, Proceedings of the Eighth (1998) International Offshore and Polar Engineering Conference, Montreal, Canada, May 24-29, 1998.

Frederking, R., 1999, The Local Pressure-Area Relation in Ship Impact with Ice, Proceedings of the 15th International Conference on Port and Ocean Engineering under Arctic Conditions, POAC'99, Vol.2, pp. 687-696, Helsinki, Finland, August 23-27, 1999.

Gagnon, R., 2004, Physical Model Experiments to Assess the Hydrodynamic Interaction Between Floating Glacial Ice Masses and a Transiting Tanker, journal of Offshore Mechanics and Arctic Engineering.

Gagnon, R. and Derradji-Aouat, A., 2006, First Results of Numerical Simulations of Bergy Bit Collision with the CCGS Terry Fox Icebreaker, the 18th International Symposium on Ice, Sapporo, Japan.

Hallquist, J.O., 2006, LS-DYNA Theory Manual 2006, Livemore Software Technology Corporation (LSTC).

Hulme, A., 1982, The Wave Forces Acting on a Floating hemisphere Undergoing Forces Periodic Oscillations, J. Fluid Mech., 121, pp. 443-463.

IACS, 2010, Requirements Concerning Polar Class, London: International Association of Classification Societies

Kendrick, A., Daley, C.G., 2000a, Derivation and Use of Formulations for Framing Design in the Polar Class Unified Requirements, Prepared for IACS Ad-hoc Group on Polar Class Ships Transport Canada, 2000.

Kendrick, A., Daley, C.G., 2000b, Unified Requirements Load Model – ‘Synthesis Approach’, Prepared for IACS Polar Rules Harmonization, Semi-Permanent Working Group, Prepared by, AMARK Inc, Montreal, and Memorial University of Newfoundland, St. John’s.

Kendrick, A., Daley, C.G. Quinton, B., 2009, Scenario-Based Assessment of Risks to Ice Class Ships, Offshore Technology Conference , Houston, Texas, USA, 4–7 May 2009, OTC 20002.

Kennedy, J., 2012, Personal communications.

Korsmeyer, F. T., and Sclavounos, P. D., 1989, The Large-Time Asymptotic Expansion of the Impulse Response Function for a Floating Body, *Appl. Ocean. Res.*, 11(2), pp. 75-88.

Kwak, M., Choi, J., Park, S., Kang, J., 2006, Strength Assessment for Bow Structure of Arctic Tanker (107k) under Ship-Ice Interaction, Daewoo Shipbuilding & Marine Engineering Co., LTD.

Lee, S., Lee, I., Baek, Y., Couty, N., Goff, S., and Quenez, J., 2007, Membrane-Type Carrier Side Collision with Iceberg Effect of Impact Conditions on Structural Response Through Sensitivity Analysis

Liapis, S. J., 1986, Time-Domain Analysis of Ship Motions, Phd thesis, University of Michigan.

Liu, Z., Amdahl, J., and Loset, S., 2009, Numerical Simulation of Collision between Ships and Icebergs, Proceedings of the 20th International Conference on Port and Ocean Engineering under Arctic Conditions, Lulea, Sweden, June 9-12, 2009.

LSTC, 2007a, LS-DYNA Keyword User's Manual Volume I, Version 971, 2007, Livermore Software Technology Corporation.

LSTC, 2007b, LS-DYNA Keyword User's Manual Volume II, Version 971, 2007, Livermore Software Technology Corporation.

LSTC, 2010, LS-DYNA Lecture Notes, 2010, Livermore Software Technology Corporation.

Masterson, D.M., Frederking, R.M.W., Wright, B., Karna, t., and Maddock, W.P., 2007, A Revised Ice Pressure-Area Curve, Recent development of Offshore Engineering in Cold Regions, Yue (ed.), POAC-07, Dalian, China, June 27-30, 2007.

Myhre, S., 2010, Analysis of Accidental Iceberg Impacts with Membrane Tank LNG Carriers, Master's thesis, Norwegian University of Science and Technology.

Prins, H. J., 1995, Time-domain Calculations of Drift Forces and Moments, PhD thesis, Delft University of Technology.

Popov, Yu., Faddeyev, O., Kheisin, D., and Yalovlev, A., 1967, Strength of Ships Sailing in Ice, Sudostroenie Publishing House, Leningrad, Technical Translation, U.S. Army Foreign Science and Technology Center, FSTC-HT-23-96-68.

Quinton, B., 2009, Progressive Damage to a Ship's Structure Due to Ice Loading, master's thesis, Memorial University of Newfoundland.

Sierevogel, L., 1998, Time Domain Calculations of Ship Motions, PhD thesis, Delft University of Technology.

Storti, M., and D'Elia, J., 2004, Added Mass of an Oscillating Hemisphere at Very-Low and Very-High Frequencies, Transactions of the ASME, 1048/Vol. 126, 2004.

Wang, B., Yu, H., Basu, R., Lee, H., Kwon, J., Jeon, B., Kim, J., Daley, C.G., and Kendrick, A., 2008a, Structural Response of Cargo Containment Systems in LNG Carriers under Ice Loads, ICETECH 2008 Conference, Banff, Canada, July 20-23, 2008.

Wang, B., Yu, H., Basu, R., 2008b, Ship and Ice Collision Modeling and Strength Evaluation of LNG Ship Structure, Proceedings of the ASME 27th International Conference on Offshore Mechanics and Arctic Engineering, Estoril, Portugal, June 15-20, 2008.

Wang, J. and Derradji-Aouat, A., 2010a, Numerical Prediction for Resistance of Canadian Icebreaker CCGS Terry Fox in Level Ice, Report from the National Research Council's Institute for Ocean Technology, St. John's, Canada.

Wang, J. and Derradji-Aouat, A., 2010b, Ship performance in Broken Ice Floes – Preliminary Numerical Simulations, Report from the National Research Council's Institute for Ocean Technology, St. John's, Canada.

Wang, J. 2011, Personal communications.

Appendices

Appendix A: STePS2 Cluster Specifications

The STePS2 cluster used in this research has specifications as follows:

Table A-1: Head Node Hardware

Processors	
# of CPUs	2
CPU type	Intel(R) Xeon(R) E5520
Cores per CPU	4
CPU Frequency	2.27 GHz
CPU Max Turbo Frequency	2.53 GHz
CPU Cache	8 MB
CPU Address Sizes	40 bits physical, 48 bits virtual
QPI Speed	5.86 GT/s
Instruction Set	64-bit
Hyper threading	Yes and Enabled
Memory	
Total Memory	32 GB
Memory per CPU	16 GB
Memory Slots	8 per CPU (all 8 filled)
DIMM Size	2 GB
Type	DDR 3 ECC
Memory Frequency	800 MHz
Storage	
Array 1	
RAID	RAID 5
Number of disks	5
Total Storage	584 GB
Storage per disk	146 GB
Disk Type	SAS
Disk Speed	15000 RPM
RAID Controller	Hardware
Array 2	
RAID	RAID 5
Number of disks	3
Total Storage	600 GB
Storage per disk	300 GB
Disk Type	SAS
Disk Speed	15000 RPM
RAID Controller	Hardware
Operating System	
Operating System	RHEL Server 5.4 (Tikanga)
Linux Kernel	2.6.18-164
Architecture	Intel x86_64

Table A-2: Compute Node Hardware

Processors	
Same as head node except	Hyper threading not Enabled
Memory	
Total Memory	24 GB
Memory per CPU	12 GB
Memory Slots	8 per CPU (6 of 8 filled)
DIMM Size	2 GB
Type	DDR 3 ECC
Memory Frequency	1067 MHz
Storage	
RAID	RAID 0
Number of disks	4
Total Storage	584 GB
Storage per disk	146 GB
Disk Type	SAS
Disk Speed	15000 RPM
RAID Controller	Hardware
Operating System	
Operating System	Same as head node

Appendix B: DYNA's Keyword File of the Final Model

This appendix is the keyword file of the final model. The keyword file of the geometric model is not included here due to its enormous size.

```
*KEYWORD
*TITLE
Ship Ice Collision Model
$=====
$ [ ] Model Geometry
$=====
*INCLUDE geo.k
$=====
$ [ ] EXECUTION CONTROLS
$=====
$*CONTROL_MPP_DECOMPOSITION_SHOW
*CONTROL_TERMINATION
$# endtim   endcyc   dtmin   endeng   endmas
2           0       0       0       0
*CONTROL_TIMESTEP
$# dtinit   tssfacc   isdo    tslimit  dt2ms    lctm     erode    ms1st
0           0.7     0       0       0       0       0       0
$# t2msf    dt2mslc   imsc1
```

```

0          0          0

*DEFINE_CURVE

$ lcid      sidr      scla      sclo      offa      offo

1000

$          abscissa      ordinate

          0          4.15E-6

          1000          4.15E-6

*CONTROL_ENERGY

$# hgen      rwen      slnten      rylen

2          2          2          2

*CONTROL_MPP_DECOMPOSITION_METHOD

$# name

RCB

*CONTROL_MPP_IO_NOD3DUMP

*CONTROL_MPP_IO_NODUMP

$=====

$ [ ] OUTPUT CONTROLS

$=====

*DATABASE_GLSTAT

$# dt      binary      lcur      ioopt

0.1      0          0          1

*DATABASE_MATSUM

```

\$# dt	binary	lcur	ioopt
--------	--------	------	-------

0.1	0	0	1
-----	---	---	---

*DATABASE_RCFORC

\$# dt	binary	lcur	ioopt
--------	--------	------	-------

0.01	0	0	1
------	---	---	---

*DATABASE_BINARY_D3PLOT

\$# dt	lcdt	beam	npltc	psetid
--------	------	------	-------	--------

0.1	0	0	0	0
-----	---	---	---	---

\$# ioopt

0

*DATABASE_BINARY_D3THDT

\$# dt	lcdt	beam	npltc	psetid
--------	------	------	-------	--------

0.1	0	0	0	0
-----	---	---	---	---

=====

\$ [] |PART_ID|SECTION_ID|MAT_ID|EOS_ID|HG_ID|

=====

*MAT_RIGID

\$# mid	ro	e	pr	n	couple	m	alias
---------	----	---	----	---	--------	---	-------

1	7850	2.0E+11	0.3	0	0	0	
---	------	---------	-----	---	---	---	--

\$# cmo	con1	con2
---------	------	------

0	0	0
---	---	---

\$# leo or	a1	a2	a3	v1	v2	v3
------------	----	----	----	----	----	----

0 0 0 0 0 0

\$-----

*PART

\$# title

rigid ship

\$# pid	secid	mid	eosid	hgid	grav	adpopt	tmid
1	1	1	0	0	0	0	0

*SECTION_SHELL

\$# secid	elform	shrf	nip	propt	qr/irid	icomp	setyp
1	2	0.833333	2	1	0	0	1

\$# t1	t2	t3	t4	nloc	marea	idof	edgset
0.03	0.03	0.03	0.03	0	0	0	0

*PART

\$# title

deep web frame

\$# pid	secid	mid	eosid	hgid	grav	adpopt	tmid
15	15	2	0	0	0	0	0

*SECTION_SHELL

\$# secid	elform	shrf	nip	propt	qr/irid	icomp	setyp
15	2	0.833333	2	1	0	0	1

\$# t1	t2	t3	t4	nloc	marea	idof	edgset
0.03	0.03	0.03	0.03	0	0	0	0

*PART

\$# title

load carrying stringers

\$# pid	secid	mid	cosid	hgid	grav	adpopt	tmid
17	17	2	0	0	0	0	0

*SECTION_SHELL

\$# secid	elform	shrf	nip	propt	qr/irid	icomp	setyp
17	2	0.83333	2	1	0	0	1

\$# t1	t2	t3	t4	nloc	marea	idof	edgset
0.03	0.03	0.03	0.03	0	0	0	0

*PART

\$# title

bulkhead

\$# pid	secid	mid	cosid	hgid	grav	adpopt	tmid
25	25	2	0	0	0	0	0

*SECTION_SHELL

\$# secid	elform	shrf	nip	propt	qr/irid	icomp	setyp
25	2	0.83333	2	1	0	0	1

\$# t1	t2	t3	t4	nloc	marea	idof	edgset
0.03	0.03	0.03	0.03	0	0	0	0

*PART

\$# title

deck

\$# pid	secid	mid	eosid	hgid	grav	adpopt	tmid
31	31	2	0	0	0	0	0

*SECTION_SHELL

\$# secid	elform	shrf	nip	propt	qr/irid	icomp	setyp
31	2	0.833333	2	1	0	0	1

\$# t1	t2	t3	t4	nloc	marea	idof	edgset
0.03	0.03	0.03	0.03	0	0	0	0

*PART

\$# title

hull

\$# pid	secid	mid	eosid	hgid	grav	adpopt	tmid
70	70	2	0	0	0	0	0

*SECTION_SHELL

\$# secid	elform	shrf	nip	propt	qr/irid	icomp	setyp
70	2	0.833333	2	1	0	0	1

\$# t1	t2	t3	t4	nloc	marea	idof	edgset
0.03	0.03	0.03	0.03	0	0	0	0

*PART

\$# title

bow

\$# pid	secid	mid	eosid	hgid	grav	adpopt	tmid
---------	-------	-----	-------	------	------	--------	------

73	73	2	0	0	0	0	0
----	----	---	---	---	---	---	---

*SECTION_SHELL

\$#	secid	elform	shrf	nip	propt	qr/irid	icomp	setyp
73		2	0.83333	2	1	0	0	1
\$#	t1	t2	t3	t4	nloc	marea	idof	edgset
0.022		0.022	0.022	0.022	0	0	0	0

*PART

\$# title

lce

\$#	pid	secid	mid	eosid	hgid	grav	adpopt	tmid
170		170	170	0	0	0	0	0

\$-----

*MAT_ADD_EROSION

\$#	mid	excl	mxpres	mneps	effeps	voleps	numfip	nes
170		0	0	0	0	0.9	1	1
\$#	mnpres	sigp1	sigvm	mxeps	epssh	sigth	impulse	failtm
0		0	0	0	0	0	0	0

*MAT_CRUSHABLE_FOAM

\$#	mid	ro	e	pr	lcid	tsc	damp
170		900	5.0E+9	0.003	170	8.0E+8	0

*DEFINE_CURVE

\$#	lcid	sidr	sfa	sfo	offa	offo	dattyp
-----	------	------	-----	-----	------	------	--------

170 0 0 0 0 0 0

\$# a1 o1
0 1.5e6
0.02 1.5e6
0.03 1.5e6
0.04 1.5e6
0.05 1.5e6
0.065 1.5e6
0.075 3e6
0.1 3e6
0.5 3e6
0.8 3e6
0.89 3e6

*SECTION_SOLID

\$# secid elform aet

170 1 0

\$-----

*PART

\$# title

rigid ice

\$# pid secid mid eosid hgid grav adpopt tmid

171 171 171 0 0 0 0 0

*MAT_RIGID

\$#	mid	ro	e	pr	n	couple	m	alias
-----	-----	----	---	----	---	--------	---	-------

171	900		5.0E+9	0.003	0	0	0	
-----	-----	--	--------	-------	---	---	---	--

\$#	cmo	con1	con2
-----	-----	------	------

1	7	7	
---	---	---	--

\$#	lco	or	a1	a2	a3	v1	v2	v3
-----	-----	----	----	----	----	----	----	----

0	0		0	0	0	0	0	0
---	---	--	---	---	---	---	---	---

*SECTION_SOLID

\$#	secid	elform	aet
-----	-------	--------	-----

171	1		0
-----	---	--	---

\$-----

*SET_PART_LIST

\$#	sid	da1	da2	da3	da4	solver
-----	-----	-----	-----	-----	-----	--------

1	0	0	0	0	0	MECH
---	---	---	---	---	---	------

\$#	pid1	pid2	pid3	pid4	pid5	pid6	pid7	pid8
-----	------	------	------	------	------	------	------	------

15	17		25	73	0	0	0	0
----	----	--	----	----	---	---	---	---

*SET_PART_LIST

\$#	sid	da1	da2	da3	da4	solver
-----	-----	-----	-----	-----	-----	--------

2	0	0	0	0	0	MECH
---	---	---	---	---	---	------

\$#	pid1	pid2	pid3	pid4	pid5	pid6	pid7	pid8
-----	------	------	------	------	------	------	------	------

170	171		0	0	0	0	0	0
-----	-----	--	---	---	---	---	---	---

*SET_PART_LIST

\$# sid	da1	da2	da3	da4	solver		
3	0	0	0	0	MECH		
\$# pid1	pid2	pid3	pid4	pid5	pid6	pid7	pid8
170	0	0	0	0	0	0	0

*SET_PART_LIST

\$# sid	da1	da2	da3	da4	solver		
4	0	0	0	0	MECH		
\$# pid1	pid2	pid3	pid4	pid5	pid6	pid7	pid8
1	15	17	25	31	70	73	0

\$=====

\$ [] CONTACTS

\$=====

*CONTACT_INTERIOR

\$# psid

3

*CONTACT_AUTOMATIC_SINGLE_SURFACE

\$# cid							title
\$# ssid	msid	sstyp	mstyp	sboxid	mboxi	spr	mpr
0	0	0	0	0	0	1	1
\$# fs	fd	dc	vc	vdc	penchk	bt	dt
0	0	0	0	0	0	0	1.0E20
\$# sfs	sfm	sst	mst	sfst	sfmt	fsf	vsf

1	1	0	0	1	1	1	1
\$# soft	sofsc1	lcidab	maxpar	sbopt	depth	bsort	frcfreq
1	0.1	0	1.025	2	2	0	1

*CONTACT_FORCE_TRANSDUCER

\$# cid							title
\$# ssid	msid	sstyp	mstyp	sboxid	mboxi	spr	mpr
1	2	2	2	0	0	1	1
\$# fs	fd	dc	vc	vdc	penchk	bt	dt
0	0	0	0	0	0	0	1.0E20
\$# sfs	sfm	sst	mst	sfst	sfmt	fsf	vsf
1	1	0	0	1	1	1	1

=====

\$ [] BC's + IC's + BODY LOAD + FORCE FIELDS

=====

*CONSTRAINED_EXTRA_NODES_NODE

\$# pid	nid
1	500000
1	500001
1	500002
1	500005
1	500006

*DEFINE_COORDINATE_NODES

\$# cid	n1	n2	n3	flag	dir		
1	500000	500001	500002	1	X		

*ELEMENT_MASS_PART_SET

\$# psid	add	mass	finmass				
4	0	0	3.1E+6				

\$-----SHIP-----

*INITIAL_VELOCITY_GENERATION

\$# sid/pid	styp	omega	vx	vy	vz	ivatn	icid
4	1	0	4	0	0	0	0

\$# xc	yc	zc	nx	ny	nz	phase	iridid
0	0	0	0	0	0	0	0

\$=====

*DEFINE_CURVE_FUNCTION

\$# lcid	sidr	sfa	sfo	offa	offo	dattyp		
3	0	1	1	0	0	0		

\$# function

-682821934*DZ(500000)

*LOAD_NODE_POINT

\$# nid	dof	lcid	sf	cid	m1	m2	m3
500000	3	3	1	0	0	0	0

*DEFINE_CURVE_FUNCTION

\$# lcid	sidr	sfa	sfo	offa	offo	dattyp		

```

5          0          1          1          0          0          0

$# function
-2.9E+07.29*AX(500000)
*LOAD_NODE_POINT
$# nid      dof      lcid      sf      cid      m1      m2      m3
500000     5        5        1        0        0        0        0
*DEFINE_CURVE_FUNCTION
$# lcid     sidr     sfa     sfo     offa     offo     dattyp
6          0        1        1        0        0        0

$# function
-1.8E+0722.13*AY(500000)
*LOAD_NODE_POINT
$# nid      dof      lcid      sf      cid      m1      m2      m3
500000     6        6        1        0        0        0        0
$-----
*DAMPING_PART_MASS_SET
$# psid     lcid     sf      flag
4          10      1        1
$# stx      sty      stz      srx      sry      srz
0          0        0.30964  0.0832  0.4639  0
*DEFINE_CURVE
$# lcid     sidr     sfa     sfo     offa     offo     dattyp

```

10 0 0 0 0 0 0

\$ abscissa ordinate

\$# a1 o1

0 0

1 1

100 1

*END



